Antagonism of PP2A is an independent and conserved function of HIV-1 Vif and causes cell cycle arrest

Sara Marelli[1,2], James C Williamson[1,2], Anna V Protasio[1,2], Adi Naamati[1,2], Edward JD Greenwood[1,2], Janet E Deane[3,4], Paul J Lehner[1,2], Nicholas J Matheson[1,2,*]

1. Department of Medicine, University of Cambridge, UK
2. Cambridge Institute for Therapeutic Immunology and Infectious Disease (CITIID), University of Cambridge, UK
3. Department of Clinical Neuroscience, University of Cambridge, UK
4. Cambridge Institute for Medical Research (CIMR), University of Cambridge, UK

*Correspondence: njm25@cam.ac.uk.

Abstract

The seminal description of cellular restriction factor APOBEC3G and its antagonism by HIV-1 Vif has underpinned two decades of research on the host-virus interaction. As well as APOBEC3G and its homologues, however, we have recently discovered that Vif is also able to degrade the PPP2R5 family of regulatory subunits of key cellular phosphatase PP2A (PPP2R5A-E) (Greenwood et al., 2016; Naamati et al., 2019). We now identify amino acid polymorphisms at positions 31 and 128 of HIV-1 Vif which selectively regulate the degradation of PPP2R5 family proteins. These residues covary across HIV-1 viruses *in vivo*, favouring depletion of PPP2R5A-E. Through analysis of point mutants and naturally occurring Vif variants, we further show that degradation of PPP2R5 family subunits is both necessary and sufficient for Vif-dependent G2/M cell cycle arrest. Antagonism of PP2A by HIV-1 Vif is therefore independent of APOBEC3 family proteins, and regulates cell cycle progression in HIV-infected cells.

Introduction

The canonical function of HIV-1 Vif is to recruit the cellular restriction factor APOBEC3G for CUL5 E3 ligase and ubiquitin-proteasome-dependent degradation in infected cells, preventing APOBEC3G encapsidation and enhancing virion infectivity (Conticello et al., 2003; Kobayashi et al., 2005; Marin et al., 2003; Mehle et al., 2004; Sheehy et al., 2002; Sheehy et al., 2003; Stopak et al., 2003; Yu et al., 2003). This interaction is very likely to be important *in vivo*, because the ability of Vif to antagonise APOBEC3G and its homologues is broadly conserved across lentiviral phylogeny, and has driven co-evolution of the mammalian APOBEC3 family (Compton et al., 2013; Nakano et al., 2017).

The other cell biological phenotype associated with Vif in multiple studies is the induction of G2/M cell cycle arrest (DeHart et al., 2008; Evans et al., 2018; Izumi et al., 2010; Sakai et al., 2006; Wang et al., 2007; Zhao et al., 2015). Vif-dependent cell cycle arrest does not require expression of APOBEC3 family proteins, but is reliant on lysine-48 ubiquitination and the same CUL5 E3 ligase complex recruited by Vif to deplete APOBEC3G (DeHart et al., 2008). It has therefore been suspected to reflect ubiquitination and degradation of an unknown cellular factor involved in cell cycle progression (DeHart et al., 2008). Why only certain HIV-1 Vif variants mediate this effect (Evans et al., 2018; Zhao et al., 2015), and how widely conserved it is across the lentiviral lineage, have remained unclear.

We have recently discovered that, in addition to APOBEC3 family proteins, Vif is also able to degrade the B56 family of regulatory subunits of the ubiquitous heterotrimeric serine-threonine phosphatase PP2A (PPP2R5A-E) in HIV-1-infected CEM-T4 T cells (Greenwood et al., 2016) and primary human CD4+ T cells (Naamati et al., 2019). This ability (illustrated in **Figure 1A**) is shared by Vif variants from diverse primate and non-primate lentiviruses (Greenwood et al., 2016), suggesting a beneficial effect on viral replication *in vivo*. In theory, however, depletion of PPP2R5A-E could be dependent on or secondary to the phylogenetically conserved ability of Vif to antagonise APOBEC3 family proteins.

53 To demonstrate that these functions are autonomous and have therefore been independently
54 selected, we now screen a library of rationally designed Vif point mutants, and identify amino
55 acid substitutions at residues 31 and 128 which clearly separate APOBEC3 and PPP2R5
56 family protein depletion. We further show that antagonism of PP2A explains the ability of Vif
57 to cause cell cycle arrest, and that this requires efficient depletion of all PPP2R5 family
58 subunits. Naturally occurring polymorphisms of residues 31 and 128 correlate with the ability
59 of HIV-1 Vif variants to cause cell cycle arrest, and reveal evidence of selection pressure for
60 PPP2R5A-E depletion *in vivo*.

Results

Flow cytometric screen identifies mutations in HIV-1 Vif which separate PPP2R5B and APOBEC3G depletion

To determine whether antagonism of PPP2R5 and APOBEC3 family proteins are independent functions of Vif, we first used the published structure of the Vif-CUL5 complex (Guo et al., 2014) to construct a library of 34 Vif variants with point mutations in solvent-exposed residues, focussing predominantly on regions distant from known APOBEC3 family protein interaction interfaces (**Figure 1B, Figure 1 – figure supplement 1A**, residues highlighted in yellow). None of these mutations is predicted to cause protein misfolding, nor interfere with the interactions between Vif and other members of the Vif-CUL5 E3 ligase complex (CBF-β, CUL5, ELOB and ELOC).

Amongst the five PPP2R5 family subunits, we previously showed that depletion of PPP2R5B is most conserved across Vif variants from HIV-1/2 and the non-human primate lentiviruses (Greenwood et al., 2016). We therefore transfected our library into HEK 293T cells (293Ts) stably expressing HA-tagged PPP2R5B or APOBEC3G, and used flow cytometry to quantify PPP2R5B and APOBEC3G depletion by each Vif variant (**Figure 1–figure supplement 1B-C** and **Figure 1–figure supplement 2A-C**). As well as indicating preserved APOBEC3 family substrate recruitment, the ability to deplete APOBEC3G served as a control for unanticipated effects on Vif expression or stability, or assembly of the Vif-CUL5 complex.

We discovered several Vif mutants to be defective for PPP2R5B depletion (**Figure 1C**). Amongst these, some mutations affected residues known to be required for depletion of APOBEC3G (K26, Y44, W70) (Letko et al., 2015) or APOBEC3C/F (R15) (Letko et al., 2015; Nakashima et al., 2016) (**Figure 1D** and **Figure 1–figure supplement 2C**). Conversely, Vif variants with mutations in residues Y30/I31, R33/K34 and I128 were defective for PPP2R5B depletion, yet retained the ability to antagonise APOBEC3G (**Figure 1C-E**). These residues are grouped in three similarly orientated patches on the Vif surface (**Figure 1B**, residues

highlighted in red). Mutations of residues I128, I31 and R33/K34 were therefore selected for further characterisation.

Residues 128 and 31 of HIV-1 Vif differentially regulate APOBEC3 and PPP2R5 family protein depletion

Vif recruits different APOBEC3 family members for degradation using distinct binding surfaces (Binka et al., 2012a; Chen et al., 2009; Dang et al., 2009; Gaddis et al., 2003; Harris and Anderson, 2016; He et al., 2008; Letko et al., 2015; Mehle et al., 2007; Nakashima et al., 2016; Ooms et al., 2016; Richards et al., 2015; Russell and Pathak, 2007; Simon et al., 2005b; Yamashita et al., 2008), and Vif variants from HIV-1/2 and the non-human primate lentiviruses differ in their abilities to deplete different PPP2R5 family subunits (Greenwood et al., 2016). We therefore sought to determine whether the mutations we found to separate depletion of PPP2R5B and APOBEC3G have similar effects on other family members. To avoid the possibility of over-expression artefacts, we focussed on endogenous APOBEC3 and PPP2R5 family members expressed in CEM-T4 T cells (CEM-T4s).

First, we transduced CEM-T4s with a panel of Vif mutants specifically lacking the ability to deplete PPP2R5B, and examined levels of PPP2R5D by immunoblot (**Figure 2A**). Together with mutations in residues I31, I128 and R33/K34, a mutation in Y44A (also defective for APOBEC3G depletion) was included as a control. As expected WT Vif was able to fully deplete PPP2R5D (lane 3). Conversely, mutations in residues I128, I31, R33/K34 and Y44 all restored PPP2R5D levels (lanes 4-9). Interestingly, the I128A (lane 4) and Y44A (lane 9) mutations only showed a partial rescue, suggesting a differential effect on different PPP2R5 subunits (PPP2R5B vs PPP2R5D). In addition, mutations in residues R33/K34 (lanes 7-8) were associated with lower levels of Vif expression (**Figure 2A**).

Validated antibodies capable of detecting and differentiating endogenous levels of all APOBEC3 and PPP2R5 family proteins are not available. We therefore evaluated the activity of a similar panel of Vif mutants using a tandem mass tag (TMT)-based functional proteomic

approach (**Figure 2B**). CEM-T4 cells were transduced with different Vif mutants at a multiplicity of infection (MOI) of 3 (range 94.1-98.7% transduced cells), then subjected to whole cell proteome analysis after a further 48 hr.

In total, we identified 8,781 proteins (**Figure 2–source data 1**), including all 5 PPP2R5 family subunits (PPP2R5A/B/C/D/E) and 5 out of 7 APOBEC3 family members (B/C/D/F/G; not A/H). This concords with previous data suggesting that APOBEC3A is restricted to myeloid cells (Berger et al., 2011; Koning et al., 2009; Peng et al., 2007; Refsland et al., 2010), and neither APOBEC3A nor APOBEC3H are expressed in CCRF-CEM cell lines at the mRNA level (Refsland et al., 2010). APOBEC3B is not antagonised by Vif (Doehle et al., 2005; Greenwood et al., 2016; Hultquist et al., 2011; Naamati et al., 2019), and is therefore not considered further.

As expected, all Vif mutants tested were defective for PPP2R5B depletion, and the Y44A mutant was also defective for APOBEC3G depletion (**Figure 2C-D**). In addition, and consistent with our immunoblot analysis (**Figure 2A**), substitutions of I128 led to loss of activity against PPP2R5A, with relatively preserved activity against PPP2R5C-E. Conversely, substitution of I31 led to a reciprocal pattern, with loss of activity against PPP2R5C-E, but relatively preserved activity against PPP2R5A. Substitutions of R33/K34 led to loss of activity against all PPP2R5 subunits, but were again associated with lower levels of Vif expression (**Figure 2–figure supplement 1**), and accompanied by partial loss of activity against APOBEC3 family proteins, particularly APOBEC3F. In conclusion, therefore, mutations in residues 128 and 31 separate PPP2R5 and APOBEC3 family depletion without affecting Vif stability, and differentially regulate the 5 PPP2R5 family members.

Depletion of PPP2R5 family subunits is necessary for Vif-dependent cell cycle arrest

We previously showed that expression of Vif results in extensive remodelling of the phosphoproteome in HIV-infected cells, including activation of the aurora kinases AURKA and AURKB, effects we attributed to PP2A antagonism (Greenwood et al., 2016; Naamati et al.,

2019). As expected, transduction of CEM-T4s with WT Vif resulted in increased AURKA/B T loop phosphorylation (**Figure 3A**, lane 3). Conversely, Vif mutants with impaired ability to antagonise PPP2R5 family subunits were unable to trigger AURKA/B phosphorylation (**Figure 3A**, lanes 4-7).

Together with APOBEC3 family antagonism, it has been known for >10 years that certain Vif variants (including NL4-3 Vif) are also able to induce G2/M cell cycle arrest, and that this is dependent on CUL5 E3 ligase recruitment and the ubiquitin-proteasome system (DeHart et al., 2008; Evans et al., 2018; Izumi et al., 2010; Sakai et al., 2006; Wang et al., 2007; Zhao et al., 2015). The Vif substrate explaining this phenomenon has, however, remained obscure.

Since both PP2A-B56 (PP2A heterotrimers incorporating one of the B56 family of regulatory subunits, PPP2R5A-E) and aurora kinases are required to coordinate mitotic progression (Foley et al., 2011; Grallert et al., 2015; Nasa and Kettenbach, 2018; Vallardi et al., 2019), we hypothesised that depletion of PPP2R5 family subunits may explain Vif-dependent cell cycle arrest, and that Vif mutants with impaired activity against PPP2R5 family subunits may also be defective for this phenotype. To test this hypothesis, we first interrogated our proteomic dataset. As predicted, WT Vif led to elevated levels of cyclin B1, indicative of G2/M arrest (**Figure 3B**). Conversely, elevation of cyclin B1 was reduced or abolished in the presence of Vif mutants lacking the ability to deplete PPP2R5 family subunits.

To confirm this result and formally evaluate cell cycle progression, we measured DNA content of CEM-T4s 48 hrs after transduction with WT or mutant Vif variants. Again, WT Vif, but not Vif mutants lacking the ability to deplete PPP2R5 subunits, caused G2/M arrest (**Figure 3C-D**). As a control, 2 other Vif mutants (F39A and D61A) which retained the ability to antagonise PPP2RB (**Figure 1–figure supplement 2A**), also retained the ability to cause cell cycle arrest (**Figure 3–figure supplement 1**).

In addition to APOBEC3 and PPP2R5 family proteins, we recently showed that NL4-3 Vif is also able to target FMR1 and DPH7 (Naamati et al., 2019). Both I128A and I128D point

mutants retain the ability to deplete these proteins (**Figure 3–figure supplement 2**), but are unable to mediate cell cycle arrest. Depletion of PPP2R5 family subunits, but not other Vif substrates, is therefore required for Vif-dependent aurora kinase activation and G2/M cell cycle arrest.

Depletion of PPP2R5 family subunits is sufficient to cause cell cycle arrest

Consistent with PPP2R5A-E depletion by Vif, inhibition of PP2A with okadaic acid causes G2/M cell cycle arrest in CEM-T4s (**Figure 4–figure supplement 1A**). However, whilst relatively specific for PP2A over other cellular phosphatases, okadaic acid does not distinguish individual PPP2R5 family subunits, nor separate PP2A-B56 activity from the activity of other PP2A heterotrimers incorporating regulatory subunits from different families (Swingle et al., 2007).

Since Vif-dependent cell cycle arrest is abrogated by point mutations which rescue quite distinct PPP2R5 subunits (compare **Figure 2C** and **Figure 3D**), some functional redundancy between the different B56 family members seems likely. Indeed, all PPP2R5 family subunits share a well conserved substrate-binding pocket (Hertz et al., 2016; Wang et al., 2016), and previous studies have suggested functional equivalence in mitosis (Foley et al., 2011; Lee et al., 2017). Conversely, another more recent study suggested topological restriction of PPP2R5 subunit activity within cells (Vallardi et al., 2019). We therefore sought to test the requirement for different PPP2R5 subunits for cell cycle progression using combinatorial knockdowns. To permit this approach, we used HeLa cells (HeLas) as a model system.

First, we confirmed that, as in CEM-T4s, expression of WT NL4-3 Vif in HeLas causes cell cycle arrest (**Figure 4–figure supplement 1B**). Next, we transfected these cells with siRNA targeting individual PPP2R5 subunits, or a pool of siRNA simultaneously targeting all subunits (same total siRNA concentration). Strikingly, we only observed cell cycle arrest when all subunits were knocked down together (**Figure 4A-B**, “pool”). Indistinguishable results were

seen for 2 independent panels of PPP2R5 family subunit siRNAs, and efficiency of siRNA knockdown was confirmed by qRT-PCR (**Figure 4–figure supplement 1C**).

To confirm that knockdown of all PPP2R5 subunits is necessary for cell cycle arrest, we repeated the experiment using pools of siRNA targeting 4 out of 5 PPP2R5 subunits ("minus one"). Again, and with the exception of PPP2R5B, cell cycle arrest was only observed when all subunits were knocked down together (**Figure 4C-D**). That depletion of PPP2R5B is neither sufficient (**Figure 4A-B**) nor required (**Figure 4C-D**) may reflect low expression of PPP2R5B in HeLas (Geiger et al., 2012), consistent with our qRT-PCR data (data not shown). Interestingly, near-identical results were previously reported from RPE1 cells (Lee et al., 2017).

Finally, knockdown of FMR1 and DPH7 (**Figure 4–figure supplement 2**) did not cause cell cycle arrest. Taken together, these observations therefore explain why efficient depletion of all PPP2R5 subunits is required to cause cell cycle arrest, and why Vif variants with impaired activity against any PPP2R5 subunit are defective for this phenotype.

Naturally occurring Vif variants phenocopy I31 and I128 point mutants

The ability to cause G2/M cell cycle arrest is known to vary between naturally occurring HIV-1 Vif variants from clade B viruses (such as NL4-3 and HXB2), as well as viruses from other clades (Evans et al., 2018; Zhao et al., 2015). We therefore examined conservation of residues 31, 33/34 and 128 across 2,171 clade B HIV-1 Vif sequences available from the Los Alamos National Laboratory Web Alignments database (**Figure 5A**). Similar results were obtained when 3,412 Vif sequences from all (any clade, including B) non-recombinant HIV-1 M groups viruses were considered (**Figure 5–figure supplement 1**).

Interestingly, residues 31 (I or V), 33 (K, G or R) and 128 (I or R, or less commonly L or V) all showed obvious polymorphism, with NL4-3 Vif encoding the commonest amino acids at positions 31 (I) and 128 (I), and the second commonest amino acid at position 33 (R). We therefore evaluated each of the common polymorphisms as single point mutations on a

background of NL4-3 Vif using our flow cytometric screen. Conservative substitutions in positions 31 and 128 partially impaired the ability of NL4-3 Vif to deplete PPP2R5B (I31V, I128V and I128L), whereas I128R resulted in more marked impairment (**Figure 5B**). Likewise, R33K, but not R33G, was well tolerated.

To evaluate these polymorphisms in their natural context, we tested Vif variants from two further clade B HIV-1 viruses in our flow cytometric assay: the HIV-1 reference strain HXB2 (encoding 31V, 33G and 128I), and the macrophage-tropic patient isolate YU2 (encoding 31I, 33G and 128R). As a control, we also included a Vif variant from the clade B transmitted founder virus CH470 (encoding 31I, 33K and 128I, similar to NL4-3 Vif) (**Figure 5C**). Consistent with the observed substitutions at residues 31, 33 and 128, HXB2 and YU2 Vif variants were markedly impaired for PPP2R5B depletion, whereas CH470 Vif was at least as active as NL4-3 Vif (**Figure 5D**). Depletion of APOBEC3G was preserved in each case (**Figure 5–figure supplement 2**).

To further assess the function of these variants against other APOBEC3 and PPP2R5 family members, we again adopted a TMT-based functional proteomic approach (**Figure 6A**). As well as HXB2, YU2 and CH470 Vif variants, we included NL4-3 Vif variants with corresponding point mutations at positions 31 and 128 (I31V and I128R). In practice, since residue 127 is also polymorphic, and residues 127 and 128 together overlap a critical HIV splicing silence (Madsen and Stoltzfus, 2005), we combined I128R and R127Y mutations (RI127/128YR, as found in YU2 Vif and detailed in **Figure 6–figure supplement 1**). Finally, to test the combinatorial effect of mutations in residues 31 and 128, we included an NL4-3 Vif variant encoding both I31A and RI127/128YR (Vif AYR). CEM-T4 cells were transduced with the panel of Vif variants at an MOI of 3 (range 93.9-98.4% transduced cells), then subjected to whole cell proteome analysis after a further 48 hr.

In this experiment, we identified 8,265 proteins (**Figure 6–source data 1**), including 4 out of 5 PPP2R5 family subunits (A/C/D/E) and 4 out of 7 APOBEC3 family members (B/C/D/G). As expected, CH470 Vif remained fully active against all PPP2R5 (**Figure 6B**) and APOBEC3

(**Figure 6C**) family subunits. Conversely, both YU2 and (in particular) HXB2 Vif variants were selectively impaired for PPP2R5 depletion (**Figure 6B**). In each case, the differential pattern of PPP2R5 family subunit depletion mirrored the effects of corresponding point mutations of residue 31 (HXB2 and NL4-3 I31V, mainly affecting PPP2R5C-E) or 128 (YU2 and NL4-3 RI127/128YR, mainly affecting PPP2R5A). Interestingly, whilst qualitatively similar to the I31A, I128A and I128D Vif mutants evaluated earlier, Vif variants with these naturally occurring polymorphisms were less severely impaired (compare **Figure 2C** with **Figure 6B**).

As a functional readout, we tested the ability of the same panel of Vif variants to cause cell cycle arrest. Consistent with previous reports (Evans et al., 2018; Zhao et al., 2015) and correlating with their impaired activity against PPP2R5 family subunits, HXB2 and NL4-3 I31V Vif variants were unable to cause cell cycle arrest (**Figure 6D** and **Figure 6–figure supplement 3**). Similarly, the potency of YU2 and NL4-3 RI127/128YR Vif variants was greatly reduced, but not abolished. Naturally occurring polymorphisms at residues 31 and 128 therefore modulate the ability of Vif to deplete PPP2R5 family subunits, and explain why some HIV-1 Vif variants are unable to cause cell cycle arrest.

Combined I31 and I128 mutations abolish PPP2R5 family subunit depletion and rarely occur in nature

Unlike individual mutations of residues 31 or 128, combined I31A and RI127128YR mutations in NL4-3 Vif (Vif AYR) completely abolished the depletion of all PPP2R5 family subunits in our proteomic analysis (**Figure 6B**), without affecting the depletion of APOBEC3 family proteins (**Figure 6C**). Since PPP2R5B was not quantitated, we confirmed that Vif AYR was also unable to deplete this subunit by flow cytometry (**Figure 6–figure supplement 2A-B**). As expected, Vif AYR was also unable to cause cell cycle arrest (**Figure 6D**).

We sought to confirm these results in the context of viral infection by introducing the same mutations into the NL4-3-based HIV-AFMACS molecular clone (Naamati et al., 2019). This Env-deficient (single round) reporter virus encodes a SBP-ΔLNGFR cell surface streptavidin-

binding affinity tag, allowing facile one-step selection of infected cells with streptavidin-conjugated magnetic beads (Antibody-Free Magnetic Cell Sorting, AFMACS) (Matheson et al., 2014). To enable analysis of cell cycle without confounding by Vpr, a Vpr-deficient (ΔVpr) background was used.

To assess the function of Vif AYR against APOBEC3 and PPP2R5 family members during viral infection, we first adopted a TMT-based functional proteomic approach to compare mock-infected cells with cells infected with ΔVpr-Vif WT, ΔVpr-ΔVif or ΔVpr-Vif AYR viruses (**Figure 7A**). CEM-T4s were infected at an MOI of 0.5 (range 29.3-48.7% infected cells), purified using AFMACS after 48 hr (range 93.3-96.6% infected cells; **Figure 7–figure supplement 1A-B**), then subjected to whole cell proteome analysis.

In this experiment, we identified 6,297 proteins (**Figure 7–source data 1**), including 4 out of 5 PPP2R5 family subunits (A/C/D/E) but only 1 out of 7 APOBEC3 family member (C). As expected, ΔVpr-Vif WT virus (**Figure 7B**, left panel) but not ΔVpr-ΔVif virus (**Figure 7B**, middle panel) was able to deplete both APOBEC3C and PPP2R5 family proteins. Conversely, ΔVpr-Vif AYR virus (**Figure 7B**, right panel) retained the ability to deplete APOBEC3C, but was completely inactive against PPP2R5 family proteins. As a control, the Nef and Vpu target CD4 was similarly downregulated by each virus (Guy et al., 1987; Willey et al., 1992). To confirm a functional effect on PP2A, we then used these viruses to infect CEM-T4 T cells, and measured their effect on cell cycle progression. Again, only ΔVpr-Vif WT virus, but not ΔVpr-ΔVif or ΔVpr-Vif AYR viruses, was able to induce G2/M cell cycle arrest (**Figure 7C**).

If the ability of Vif to antagonise PP2A is maintained by selection pressure *in vivo*, combinations of unfavourable (less active against PPP2R5A-E) mutations in residues 31 and 128 (abolishing all PPP2R5 family subunit depletion) should be rare amongst naturally occurring HIV-1 Vif variants. Furthermore, if effects on viral fitness are synergistic, such combinations should occur less frequently than predicted by chance. We therefore examined covariance of polymorphisms of residues 31 and 128 across the clade B HIV-1 Vif sequences

295 available from the Los Alamos National Laboratory Web Alignments database (**Figure 7D**;
296 same 2,171 sequences as **Figure 5A**).

297 Amongst these sequences, 21.8% encode 31V (less active) and 33.6% encode R128 (less
298 active). By chance, combinations of 31V and 128R would therefore be expected in 7.3% of
299 sequences. Conversely, this combination is observed in only 5.8% of sequences. Whist this
300 difference appears modest, the association between these polymorphisms is highly
301 statistically significant (p=0.0003, Fisher's exact test, **Figure 7–figure supplement 2A**, left
302 panel). We observed similar, significant under-representation when we limited our analysis to
303 clade B viruses encoding combinations of 31I/V and 128I/R (**Figure 7–figure supplement**
304 **2A**, right panel), or extended it to include Vif sequences from all (any clade, including B) non-
305 recombinant HIV-1 M groups viruses (**Figure 7–figure supplement 2B-C**; same 3,412
306 sequences as **Figure 5–figure supplement 1**).

307 To distinguish functional covariance of these residues from background linkage disequilibrium
308 (co-inheritance of polymorphisms from a common ancestor), we constructed phylogenetic
309 trees of all Vif variants based on Vif (**Figure 7E**) or Nef, Gag or Env (**Figure 7–figure**
310 **supplement 3A**). Regardless of the viral protein used, viruses encoding different
311 combinations of 31/128 polymorphisms were scattered throughout the phylogeny, with no
312 obvious founder effect. Again, similar results were seen when we extended our analysis to
313 include Vif sequences from all (any clade, including B) non-recombinant HIV-1 M groups
314 viruses (**Figure 7–figure supplement 3B**).

315 Taken together, these data therefore provide evidence of a functional interaction between
316 residues 31/128, and suggest significant *in vivo* selection pressure to maintain the ability of
317 Vif to antagonise PP2A.

Discussion

The study of cellular proteins and processes targeted by HIV has provided critical insights into the host-virus interaction. Typically, these targets have been identified piecemeal, using candidate approaches. In contrast, we have recently adopted unbiased proteomic approaches to identify novel substrates of HIV accessory proteins (Greenwood et al., 2016; Greenwood et al., 2019; Matheson et al., 2015; Naamati et al., 2019). A key challenge is now to determine the biological significance of these targets for HIV-infected cells: both *whether* they are important, and *why* they are important.

In this study, we sought to address these questions for Vif targets PPP2R5A-E. By demonstrating that depletion of PPP2R5 family subunits by Vif is separable from targeting of APOBEC3 family proteins, we formally prove that PP2A antagonism is neither required for, nor an epiphenomenon of, APOBEC3 family protein depletion. Combined with evidence of conservation across HIV-1 viruses and the broader lentiviral lineage (Greenwood et al., 2016), these observations provide strong genetic evidence for the importance of PPP2R5 depletion by Vif *in vivo*.

Strikingly, the critical residues for PPP2R5 depletion identified in our screen included several previously determined to be important for Vif-dependent cell cycle arrest in other, independent studies (31, 33, 44) (DeHart et al., 2008; Zhao et al., 2015). As well as residues required for CUL5 complex assembly (114 and 145), several additional residues (14, 36, 48 and 40) were implicated in the same studies. Amongst these, a K36A point mutant showed an intermediate effect on PPP2R5B depletion in our screen (**Figure 1–figure supplement 2A**). The other residues were not tested, because we focussed on regions of Vif not known to be important for depletion of APOBEC3 family proteins, and residues with solvent-exposed side chains unlikely to lead to structural disruption.

We were initially puzzled because some Vif point mutants were markedly impaired in their ability to cause cell cycle arrest, yet retained the ability to deplete at least some PPP2R5 family

subunits. Furthermore, the ability of Vif to cause cell cycle arrest did not appear to correlate with depletion of any one, specific PPP2R5 subunit. In fact, because efficient depletion of all PPP2R5 subunits is required to halt cell cycle progression, these are not paradoxes at all. This same model also suggests explanations for two related phenomena.

First, expression of HIV-1 Vif in mouse or COS cells results in depletion of PPP2R5D, but does not cause cell cycle arrest (Evans et al., 2018). As with Vif point mutants and naturally occurring variants in human cells, it seems likely that another PPP2R5 subunit escapes depletion in these species-mismatched cells. Second, we previously found the ability of Vif to antagonise at least some PPP2R5 subunits to be widely conserved (Greenwood et al., 2016), but the ability to cause cell cycle arrest is variable amongst HIV-1 Vif variants (Evans et al., 2018; Zhao et al., 2015). Since efficient depletion of all expressed PPP2R5 subunits is required to cause cell cycle arrest, escape of even a single subunit allows cell cycle to progress.

Amongst all HIV-1 Vif sequences analysed here, the commonest single combination or residues at positions 31 and 128 was 31I/128I, accounting for approximately 30% of Vif variants. Most of these sequences also encode 33R or 33K and, like NL4-3 and CH470 Vif, are therefore expected to efficiently degrade PPP2R5A-E, and cause cell cycle arrest. Conversely, only approximately 5% encode 31V/128R, and are therefore expected to be severely impaired for PPP2R5A-E degradation. It is likely that most of the remaining Vif variants, like YU2 and HXB2, are active against at least some PPP2R5 family members, but may be variably attenuated in their ability to cause cell cycle arrest. Interestingly, naturally occurring Vif variants have also been shown to exhibit a spectrum of activity against APOBEC3 family proteins, including variants which fail to neutralise one or more APOBEC3 family proteins (Binka et al., 2012b; Iwabu et al., 2010; Mulder et al., 2008; Simon et al., 2005a).

Mechanistically, hyperphosphorylation of aurora kinase substrates is expected to contribute significantly to Vif-dependent cell cycle arrest (Foley et al., 2011). Nonetheless, PP2A is a

371 "master regulator" of cell cycle (Wlodarchak and Xing, 2016), and depletion of PPP2R5A-E by
372 Vif causes widespread remodelling of the phosphoproteome, implying activation of multiple
373 kinases (Greenwood et al., 2016). Consistent with this, Vif-dependent cell cycle arrest was
374 previously shown to require TP53 (Izumi et al., 2010), and several studies have identified
375 upstream regulation of TP53 by PP2A in different systems (Ajay et al., 2010; Li et al., 2002;
376 Yang and Phiel, 2010).

377 Many RNA and DNA viruses cause and are thought to benefit from cell cycle arrest (Bagga
378 and Bouchard, 2014). In HIV infection, G2/M cell cycle arrest was first attributed to Vpr (He et
379 al., 1995; Jowett et al., 1995; Rogel et al., 1995), which remains better known for this function.
380 Early studies suggested a positive effect of G2/M arrest on transcription from the HIV-1 LTR
381 (Goh et al., 1998; Gummuluru and Emerman, 1999), but more recent results have raised the
382 possibility that cell cycle arrest may be secondary to another Vpr-dependent process, such as
383 antagonism of innate immunity (Laguette et al., 2014). Nonetheless, targeting of the same cell
384 biological process by multiple viral accessory proteins is strong *a priori* evidence of biological
385 importance *in vivo*.

386 Functional redundancy with Vpr may also help explain why Vif-dependent cell cycle arrest is
387 not more strictly conserved across naturally occurring HIV-1 Vif variants. In addition, key
388 polymorphic residues which regulate PPP2R5 antagonism may be subject to balancing
389 selection pressures. First, the requirement to maintain the Exonic Splicing Silencer of Vpr
390 (ESSV) at the RNA level limits the sequence variability tolerated at position 128 (Madsen and
391 Stoltzfus, 2005). Second, polymorphisms at position 31 also regulate antagonism of
392 APOBEC3H (Zhao et al., 2015). Indeed, at least in some cases, the abilities of Vif to
393 antagonise APOBEC3H and cause cell cycle arrest were found to be mutually exclusive.

394 Vif-dependent cell cycle arrest correlates with viral cytopathicity (Evans et al., 2018; Sakai et
395 al., 2006), and was reported to enhance HIV-1 replication *in vitro* in a previous study using
396 chimeric HXB2/NL4-3 Vif variants (Izumi et al., 2010). Classic experiments comparing WT and
397 Vif-deficient viruses in permissive cells often examined HXB2 (Gabuzda et al., 1992) or YU2

(Gaddis et al., 2003) viruses. Since these Vif variants are shown here to be attenuated in their activity against different PPP2R5 subunits, manifested by a reduced ability to cause cell cycle arrest, it is likely that these studies failed to fully capture the effects of PP2A antagonism on viral infection.

As importantly, the ability to assess APOBEC3-independent effects of Vif on viral fitness *in vitro* has hitherto been limited to comparisons between WT and Vif-deficient viruses on an APOBEC3-negative background, such as the CEM-SS cell line. In contrast, the point mutants identified in this study maintain the ability to antagonise APOBEC3 family proteins, and will therefore allow the assessment of Vif-dependent PP2A antagonism by the community in a full range of cell types, including primary and myeloid cells, as well as providing a mechanistic framework to interpret the results.

Materials and Methods

Key resources table

Reagent type (species) or resource	Designation	Source or reference	Identifiers	Additional information
cell line ()	CEM-T4 T cells (CEM-T4s)	NIH AIDS Reagent Program	Cat. #: 117	Also known as CEM CD4+ cells
cell line ()	HeLa cells (HeLas)	Lehner laboratory stocks	RRID: CVCL_0030	
cell line ()	HEK 293T cells (293Ts)	Lehner laboratory stocks	RRID: CVCL_0063	
antibody	Mouse monoclonal BV421-conjugated anti-CD4	BioLegend	Cat. #: 317434	Flow cytometry
antibody	Mouse monoclonal PE-conjugated anti-CD4	BD Biosciences	Cat. #: 561843	Flow cytometry
antibody	Mouse monoclonal AF647-conjugated anti-LNGFR	BioLegend	Cat. #: 345114	Flow cytometry
antibody	Mouse monoclonal FITC-conjugated anti-LNGFR	BioLegend	Cat. #: 345103	Flow cytometry
antibody	Mouse monoclonal DyLight 650-conjugated anti-HA tag	abcam	Cat. #: ab117515	Flow cytometry
antibody	Rabbit monoclonal anti-PPP2R5D	abcam	Cat. #: ab188323	Immunoblot
antibody	Mouse monoclonal anti-HIV-1 Vif	NIH AIDS Reagent Program	Cat. #: 6459	Immunoblot
antibody	Rabbit polyclonal anti-FMR1 (FMRP)	Cell Signalling Technology	Cat. #: 4317	Immunoblot
antibody	Rabbit polyclonal anti-DPH7	Atlas Antibodies	Cat. #: HPA022911	Immunoblot
antibody	Mouse monoclonal anti-β-actin	Sigma	Cat. #: A5316	Immunoblot
antibody	Mouse monoclonal anti-p97 (VCP)	Abcam	Cat. # ab11433	Immunoblot
antibody	Rabbit polyclonal anti-total AURKB	Cell Signalling Technology	Cat. #: 3094	Immunoblot
antibody	Rabbit monoclonal anti-phospho-AURK	Cell Signalling Technology	Cat. #: 2914	Immunoblot
recombinant DNA reagent	pHRSIN-SE-P2A-SBP-ΔLNGFR-W	(Matheson et al., 2014)	N/A	Used as a control and to express codon optimised Vif variants
recombinant DNA reagent	pHRSIN-SE-W-pSV40-puro	(van den Boomen et al., 2014)	N/A	Used as a control
recombinant DNA reagent	pHRSIN-S-W-pGK-puro	(Greenwood et al., 2016)	N/A	Used to express HA-tagged PPP2R5B and APOBEC3G
recombinant DNA reagent	HIV-AFMACS	(Naamati et al., 2019)	GenBank: MK435310.1	pNL4-3-ΔEnv-Nef-P2A-SBP-ΔLNGFR proviral construct
commercial assay or kit	NEBuilder HiFi DNA Assembly Cloning Kit	NEB	Cat. #: E5520S	

commercial assay or kit	Fugene 6 Transfection Reagent	Promega	Cat. #E2691	
commercial assay or kit	Lipofectamine RNAiMAX Transfection Reagent	Invitrogen	Cat. #: 18080044	
chemical compound, drug	Lenti-X Concentrator	Clontech	Cat. #: 631232	
commercial assay or kit	Dynabeads Biotin Binder	Invitrogen	Cat. #: 11047	
commercial assay or kit	S-Trap micro MS Sample Preparation Kit	Protifi	Cat. #: C02-micro	
commercial assay or kit	TMT10plex Isobaric Label Reagent Set	Thermo Scientific	Cat. #: 90110	
commercial assay or kit	Superscript III First-Strand Synthesis System	Invitrogen	Cat. #: 18080051	
software, algorithm	PyMOL Molecular Graphics System, Version 2.0	Schrödinger	RRID:SCR_006054	https://www.schrodinger.com/pymol
software, algorithm	Proteome Discoverer 2.1	Thermo Scientific	RRID: SCR_014477	
software, algorithm	R v.3.5.3	(R Core Team, 2019)	RRID: SCR_001905	https://www.R-project.org/
software, algorithm	limma	(Ritchie et al., 2015)	RRID:SCR_010943	https://bioconductor.org/packages/limma/
software, algorithm	WebLogo	(Crooks et al., 2004)	RRID:SCR_010236	http://weblogo.berkeley.edu
software, algorithm	seqinr	(Charif and Lobry, 2007)	N/A	https://cran.r-project.org/web/packages/seqinr/
software, algorithm	ggplot2	(Wickham, 2009)	RRID:SCR_014601	https://ggplot2.tidyverse.org
software, algorithm	ggtree	(Yu et al., 2018)	N/A	https://bioconductor.org/packages/release/bioc/html/ggtree.html
software, algorithm	Clustal Omega	(Sievers and Higgins, 2014)	RRID:SCR_001591	https://www.ebi.ac.uk/Tools/msa/clustalo/
software, algorithm	Prism 7.0	GraphPad	RRID:SCR_002798	

Cell culture

CEM-T4 T cells (Foley et al., 1965) were obtained directly (< 1yr) from the AIDS Reagent Program, Division of AIDS, NIAD, NIH (Dr J. P. Jacobs), and cultured at a density of $5x10^5$ to $2x10^6$ cells/ml in RPMI supplemented with 10% FCS, 100units/ml penicillin and 0.1 mg/ml streptomycin at 37℃ in 5% CO2. HeLa cells and HEK 293T cells (authenticated by STR profiling (Menzies et al., 2018; Miles et al., 2017)) were obtained from Lehner laboratory stocks and cultured in DMEM supplemented with 10% fetal calf serum (FCS), 100 units/ml penicillin

and 0.1 mg/ml streptomycin at 37℃ in 5% CO2. All cells were regularly screened and confirmed to be mycoplasma negative (Lonza MycoAlert).

Vectors for transgene expression

Sequences for Vif variants from NL4-3 (AF324493.2) , HXB2 (K03455.1), YU2 (GenBank: M93258.1) and CH470 (JX972238-JX972249) viruses were obtained from GenBank. The CH470 transmitted founder (TF) Vif sequence was inferred as previously described (Fenton-May et al., 2013; Liu et al., 2013; Parrish et al., 2013).

For co-expression of codon optimised Vif variants with EGFP, gBlocks (IDT) encoding NL4-3, HXB2, YU2 or CH470 Vif were incorporated into pHRSIN-SE-P2A-SBP-ΔLNGFR-W (Matheson et al., 2014) in place of SBP-ΔLNGFR by Gibson assembly between XhoI/KpnI sites (generating pHRSIN-SE-P2A-Vif-W vectors). In these vectors, Vif variants are expressed from the *Friend spleen focus-forming virus* (SFFV) promoter as EGFP-P2A-Vif, downstream of EGFP and a 'self-cleaving' *Porcine teschovirus-1 2A* (P2A) peptide.

Complete sequences for all gBlocks are included in **Supplementary file 1** (Codon-optimised Vif variants synthesised as gBlocks). Codon optimisation was conducted using the IDT codon optimisation tool, and sequences were verified by Sanger sequencing (Source BioScience).

The parental vector (in which EGFP and the SBP-ΔLNGFR cell surface selection marker are expressed from the SFFV promoter as EGFP-SBP-ΔLNGFR) was used here as a control. Where indicated, pHRSIN-SE-W-pSV40-puro (in which EGFP is expressed from the SFFV promoter as a single transgene) was used as an alternative control (van den Boomen et al., 2014).

To generate stable 293T cell lines for our flow cytometric screen, N-terminal 4xHA-tagged PPP2R5B and C-terminal 4xHA-tagged APOBEC3G were expressed using pHRSIN-S-W-pGK-puro exactly as previously described (Greenwood et al, 2016).

Vif mutant library construction

To generate a library of Vif point mutants, a PCR and Gibson assembly-based approach was used to modify codon-optimised NL4-3 Vif directly in pHRSIN-SE-P2A-Vif-W (**Figure 1–figure supplement 1A**).

Briefly, forward and reverse primers encoding each point mutation were designed with ~15 bp fully complementary flanking sequences. These mutation-specific primers were used in pairwise PCR reactions in conjunction with common primers complementary to the vector backbone, which was cut between XhoI/KpnI sites. The two PCR products were then assembled into the vector using the NEBuilder HiFi DNA Assembly Master Mix (NEB).

Sequences for all primers used are tabulated in **Supplementary file 1** (PCR primers for Vif mutant library construction). All sequences were verified by Sanger sequencing (Source BioScience).

HIV-1 molecular clones

HIV-AFMACS (pNL4-3-ΔEnv-Nef-P2A-SBP-ΔLNGFR; GenBank: MK435310.1) has been previously described (Naamati et al., 2019). To introduce mutations in the native NL4-3 Vif coding sequence, the same PCR and Gibson assembly-based approach developed for Vif mutant library construction was used, cutting the vector backbone between AgeI/SalI sites. Where indicated, multiple mutations were introduced sequentially.

To generate ΔVpr-Vif WT virus (lacking Vpr expression, but encoding WT Vif), a silent mutation was introduced into Vif codon 173 (AGA>AGG; both encoding Arg), eliminating the Vpr start codon in the +2 reading frame. Additional point mutations were introduced to generate ΔVpr-Vif AYR virus (lacking Vpr expression, but encoding Vif with I31A and R127Y/I128R mutations) and ΔVpr-ΔVif virus (lacking Vpr expression, and encoding two premature stop codons after the final in-frame start codon in the Vif open reading frame).

Final Vif coding sequences for each virus are included in **Supplementary file 1** (Vif coding sequences in HIV-AFMACS viruses). Sequences were verified by Sanger sequencing (Source BioScience).

Transient transfection

For the flow cytometric screen, 293T cells stably expressing HA-tagged PPP2R5B or APOBEC3G were transfected with 200 ng/well control or Vif expression vector in 24-well plates using FuGENE 6 (Promega). After 36 hr, cells were harvested with trypsin-EDTA and analysed by flow cytometry.

siRNA transfection

For RNAi-mediated knockdown, HeLa cells were transfected with custom siRNA duplexes (Sigma) using transfected using Lipofectamine RNAiMAX (Invitrogen) according to the manufacturer's instructions.

Briefly, $2x10^5$ cells/well were seeded in 6-well plates 24 hr prior to transfection with a total of 50 pmol/well siRNA (individual or pooled). Knockdown was verified by real-time PCR or immunoblot 24 hr post-transfection, and cells were re-seeded prior to cell cycle analysis 48 hr post-transfection (target 50% confluency).

All siRNA target sequences used are tabulated in **Supplementary file 1** (Target sequences for RNAi). Cells not subjected to knockdown were transfected with MISSION siRNA Universal Negative Control #1 (Sigma) at equivalent concentrations.

Viral stocks

VSVg-pseudotyped lentivector stocks were generated by co-transfection of 293Ts with pHRSIN-based lentivector, p8.91 and pMD.G at a ratio of 2:1:1 (µg) DNA and a DNA:FuGENE 6 ratio of 1 µg:3 µl. Media was changed the next day and viral supernatants harvested and filtered (0.45 µm) at 48 hr prior to concentration with Lenti-X Concentrator (Clontech) and storage at -80℃.

VSVg-pseudotyped HIV-AFMACS viral stocks were generated by co-transfection of 293Ts with HIV-AFMACS molecular clones and pMD.G at a ratio of 9:1 (µg) DNA and a

494 DNA:FuGENE 6 ratio of 1 µg:6 µl. Viral supernatants were harvested, filtered, concentrated
495 and stored as per pHRSIN-based lentivector stocks.

496 Lentivector/viral stocks were titrated by transduction/infection of known numbers of relevant
497 target cells with known volumes of stocks under standard experimental conditions, followed
498 by flow cytometry for EGFP (GFP-expressing lentivectors) or SBP-ΔLNGFR and CD4 (HIV-
499 AFMACS viruses) at 48 hr to identify the fraction of transduced/infected cells (f) containing at
500 least one transcriptionally active provirus (EGFP positive or SBP-ΔLNGFR positive/CD4 low).
501 The number of transducing/infectious units present was then calculated by assuming a
502 Poisson distribution (where $f = 1-e^{-MOI}$). Typically, a dilution series of each stock was tested,
503 and titre determined by linear regression of -ln(1-f) on volume of stock.

504 **Transductions and infections**

505 CEM-T4s or HeLas were transduced or infected by spinoculation at 800 g for 1 hr in a non-
506 refrigerated benchtop centrifuge in complete media supplemented with 10 mM HEPES.

507 **Antibody-Free Magnetic Cell Sorting (AFMACS)**

508 AFMACS-based selection of CEM-T4s using the streptavidin-binding SBP-ΔLNGFR affinity
509 tag was carried out essentially as previously described (Matheson et al., 2014; Naamati et al.,
510 2019). Briefly, $1x10^6$ CEM-T4s/condition were infected with VSV-g pseudotyped HIV-AFMACS
511 viruses at an MOI of 0.5. 48 hr post-infection, washed cells were resuspended in incubation
512 buffer (IB; Hank's balanced salt solution, 2% dialysed FCS, 1x RPMI Amino Acids Solution
513 (Sigma), 2 mM L-glutamine, 2 mM EDTA and 10 mM HEPES) at 10^7 cells/ml and incubated
514 with Dynabeads Biotin Binder (Invitrogen) at a bead-to-total cell ratio of 4:1 for 30 min at 4℃.
515 Bead-bound cells expressing SBP-ΔLNGFR were selected using a DynaMag-2 magnet
516 (Invitrogen), washed to remove uninfected cells, then released from the beads by incubation
517 in complete RPMI with 2 mM biotin for 15 min at room temperature (RT). Enrichment was
518 assessed by flow cytometry pre- and post-selection.

519 **Proteomics**

520 Sample preparation

521 For TMT-based whole cell proteomic analysis of transduced or infected CEM-T4s, washed
522 cell pellets were lysed in 50 mM HEPES pH 8 with 5% SDS followed by 10 min (30 sec on/off)
523 sonication in a Bioruptor Pico sonicator (Diagenode) at 18 °C. Lysates were quantified by BCA
524 assay (Thermo Scientific) and 25 µg (transduced CEM-T4s, experiments 1-2) or 10 µg
525 (infected and AFMACS-selected CEM-T4s, experiment 3) total protein/condition used for
526 further analysis.

527 Sample volumes were equalised with lysis buffer and proteins reduced and alkylated by
528 addition of 10mM TCEP and 20mM iodoacetamide followed by incubation at RT for 30 min,
529 protected from light. Samples were then processed using S-Trap micro columns (Protifi). To
530 each sample 10% v/v H_3PO_4 was added and samples mixed by vortexing briefly. 6 volumes
531 of 90% MeOH HEPES pH 7.1 (loading buffer) were then added and pipette-mixed before
532 loading onto columns using a vacuum manifold.

533 Samples were then washed with 4x 150 µl loading buffer. A 1:25 enzyme:protein ratio of
534 LysC/trypsin mix (Promega) was added to each column in 30 µl of 50 mM HEPES pH 8 with
535 0.1% sodium deoxycholate (SDC). Columns were placed into microcentrifuge tubes and
536 incubated for 6 hr at 37 °C in a Thermomixer S (Eppendorf) without shaking. Open tubes of
537 water were placed in empty positions and the Thermomixer lid used to minimise evaporation.

538 After incubation, peptides were eluted in three stages: 40 µl 10 mM HEPES pH 8; 35 µl 0.2%
539 formic acid (FA); then 35 µl 0.2% FA in 50% Acetonitrile (ACN). Samples were dried for a
540 short period in a vacuum centrifuge to evaporate ACN and then acidified with FA to precipitate
541 SDC. Samples were then made up to ~100 µl with water, then 600 µl ethyl acetate was added
542 and samples vortexed vigorously. After centrifugation at 15,000 g for 5 min the lower phase
543 (containing peptides) was retained and the upper phase (containing SDC and ethyl acetate)
544 was discarded.

After drying fully in a vacuum centrifuge, samples were resuspended in 21 µl 100 mM HEPES pH 8, to which was added 0.2 mg of TMT label dissolved in 9 µl ACN. After 1 hr incubation at RT samples were analysed by LCMS to ensure complete labelling, then pooled and dried by ~50% in a vacuum centrifuge. The pooled sample was made up to ~1ml in a final concentration of 0.1% triflouracetic acid (TFA) and the pH was adjusted to <2 with FA. The samples were then subjected to C18 SPE clean-up using 500 mg Sep-Pak tC18 cartridges (Waters). Columns was wetted with 1 ml ACN and equilibrated with 3 ml 0.1% TFA before loading the sample, washing with 2 ml 0.1% TFA and eluting with 250 µl 40% ACN, 250 µl 80% ACN and 250 µl 80% ACN. The eluates were dried in a vacuum centrifuge.

Off-line high pH reversed-phase (HpRP) peptide fractionation

HpRP fractionation was conducted on an Ultimate 3000 UHPLC system (Thermo Scientific) equipped with a 2.1 mm × 15 cm, 1.7 µm Kinetex EVO C18 column (Phenomenex). Solvent A was 3% ACN, Solvent B was 100% ACN, and solvent C was 200 mM ammonium formate (pH 10). Throughout the analysis solvent C was kept at a constant 10%. The flow rate was 400 µl/min and UV was monitored at 280 nm. Samples were loaded in 90% A for 10 min before a gradient elution of 0–10% B over 10 min (curve 3), 10-34% B over 21 min (curve 5), 34-50% B over 5 min (curve 5) followed by a 10 min wash with 90% B. 15 sec (100 µl) fractions were collected throughout the run. Peptide-containing fractions were orthogonally recombined into 24 (transduced CEM-T4s, experiments 1-2) or 12 (infected and AFMACS-selected CEM-T4s, experiment 3) fractions, dried in a vacuum centrifuge and stored at −20 °C prior to analysis.

Mass spectrometry

Data were acquired on an Orbitrap Fusion mass spectrometer (Thermo Scientific) coupled to an Ultimate 3000 RSLC nano UHPLC (Thermo Scientific). Solvent A was 0.1% FA and solvent B was ACN/0.1% FA. HpRP fractions were resuspended in 20 µl 5% DMSO 0.5% TFA and 10 µl injected. Fractions were loaded at 10 µl/min for 5 min on to an Acclaim PepMap C18

cartridge trap column (300 µm × 5 mm, 5 µm particle size) in 0.1% TFA. After loading, a linear gradient of 3–32% B over 3 hr was used for sample separation over a column of the same stationary phase (75 µm × 50 cm, 2 µm particle size) before washing with 90% B and re-equilibration. An SPS/MS3 acquisition was used for all samples and was run as follows. MS1: quadrupole isolation, 120,000 resolution, $5x10^5$ AGC target, 50 msec maximum injection time, ions injected for all parallelisable time. MS2: quadrupole isolation at an isolation width of m/z 0.7, CID fragmentation (NCE 35) with the ion trap scanning out in rapid mode from m/z 120, $8x10^3$ AGC target, 70 msec maximum injection time, ions accumulated for all parallelisable time. In synchronous precursor selection mode the top 10 MS2 ions were selected for HCD fragmentation (65NCE) and scanned out in the orbitrap at 50,000 resolution with an AGC target of $2x10^4$ and a maximum accumulation time of 120 msec, ions were not accumulated for all parallelisable time. The entire MS/MS/MS cycle had a target time of 3 sec. Dynamic exclusion was set to +/−10 ppm for 90 sec, MS2 fragmentation was trigged at $5x10^3$ ions.

Data processing

Spectra were searched using Mascot within Proteome Discoverer 2.2 in two rounds. The first search was against the UniProt human reference proteome, a custom HIV proteome (adjusted to include the exact protein coding sequences used) and a compendium of common contaminants (Global Proteome Machine). The second search took all unmatched spectra from the first search and searched against the human trEMBL database. The following search parameters were used. MS1 tol: 10 ppm; MS2 tol: 0.6 Da; fixed mods: carbamidomethyl (C) and TMT (N-term, K); var mods: oxidation (M); enzyme: trypsin (/P). MS3 spectra were used for reporter ion based quantitation with a most confident centroid tolerance of 20 ppm. PSM FDR was calculated using Mascot percolator and was controlled at 0.01% for ‘high’ confidence PSMs and 0.05% for ‘medium’ confidence PSMs. Normalisation was automated and based on total s/n in each channel.

All proteomics datasets described in this study will be deposited to the ProteomeXchange consortium (accessible at: http://proteomecentral.proteomexchange.org) prior to publication and are summarised in **Figure 2–source data file 1**, **Figure 6–source data file 1** and **Figure 7–source data file 1**.

Statistical analysis

Abundances or proteins/peptides satisfying at least a 'medium' FDR confidence were subjected to further analysis in Excel 2016 (Microsoft) and R v.3.6.1 (R Core Team, 2019).

For proteomic experiments 1 and 2, abundances in the 3 mock-transduced samples were used to calculate sample means ($\bar{x}$) and standard deviations (S) for each protein. Corresponding protein abundances in transduced cells were then compared with these values to determine standard scores (*t*-scores) for each condition: (X-$\bar{x}$)/S (where X represents protein abundance in the condition of interest). Significant outliers were identified by calculating two-tailed *p*-values using a *t*-distribution with 2 degrees of freedom. Illustrative *t*-score/*p*-value calculations for PPP2R5A in cells transduced with WT Vif or a control lentivector are shown in **Figure 2–figure supplement 2**.

For proteomic experiment 3, mean protein abundances in cells infected with ΔVpr-Vif WT, ΔVpr-ΔVif, or ΔVpr-Vif AYR viruses were compared with mean protein abundances in mock-infected cells. For each pair-wise comparison, a moderated *t*-test was conducted using the limma R package (Ritchie et al., 2015; Schwammle et al., 2013). Benjamini-Hochberg FDR-adjusted p values (q values) were used to control the false discovery rate.

Antibodies

Antibodies for immunoblot and flow cytometry are detailed in the **Key resources table**. Anti-HIV-1 Vif (Simon et al., 1995) was obtained from the AIDS Reagent Program, Division of AIDS, NIAID, NIH (Dr M. H. Malim).

Flow cytometry

620 Antibody staining

621 For the flow cytometric screen in 293Ts, a sub-confluent 24-well/condition was harvested with
622 trypsin-EDTA, fixed and permeabilised using the Cytofix/Cytoperm Fixation and
623 Permeabilisation Kit (BD Biosciences) according to the manufacturer's instructions.
624 Permeabilised cells were stained with AF647-conjugated rabbit anti-HA antibody (abcam) for
625 20 min at RT, washed, and analysed with an LSR Fortessa flow cytometer (BD Biosciences).
626 Doublets were excluded by comparing SSC-W with SSC-H. Depletion of HA-tagged PPP2R5B
627 or APOBEC3G was quantified by the ratio of median A4647 fluorescence in GFP+
628 (transfected, Vif+)/GFP- (untransfected, Vif-) cells for each condition.

629 For titration of HIV-AFMACS viruses, typically $2X10^5$ washed CEM-T4s were stained with
630 fluorochrome-conjugated anti-LNGFR and anti-CD4 for 15 min at 4℃ then fixed in PBS/1%
631 paraformaldehyde and analysed as above. For titration of lentivectors, GFP fluorescence was
632 quantified without antibody staining.

633 DNA content

634 For cell cycle analysis in transduced CEM-T4s and transduced/transfected HeLas, $1x10^6$
635 cells/condition (CEM-T4s) or a 50% confluent 6-well/condition (HeLas) were washed with
636 PBS, then fixed for 30 min with ice-cold 90% methanol. Fixed cells were stained with 7-AAD
637 at 25 µg/ml for 30 mins at 37 °C, then analysed with an LSR Fortessa flow cytometer (BD
638 Biosciences). Doublets were excluded by comparing SSC-W with SSC-H. The FlowJo cell
639 cycle platform was used to determine the fraction of cells in each phase of cell cycle. G2/M
640 cell cycle arrest was quantified by the ratio of cells in G2/M for each condition, compared with
641 mock-transduced/transfected cells.

642 For cell cycle analysis in CEM-T4s infected with HIV-AFMACS, cells were first stained with
643 FITC-conjugated anti-LNGFR (BioLegend), then washed, fixed and stained with 7-AAD and
644 analysed as above. G2/M cell cycle arrest was quantified by the ratio of cells in G2/M for
645 LNGFR+ (infected, HIV+)/LNGFR- (uninfected) cells for each condition.

646 **Immunoblotting**

647 Washed cell pellets were lysed in PBS/2% SDS supplemented with Halt Protease and
648 Phosphatase Inhibitor Cocktail (Thermo Scientific) and benzonase (Sigma) for 10 min at RT.
649 Post-nuclear supernatants were heated in Laemelli Loading Buffer for 5 min at 95 ℃,
650 separated by SDS-PAGE and transferred to Immobilon-P membrane (Millipore). Membranes
651 were blocked in PBS/5% non-fat dried milk (Marvel)/0.2% Tween and probed with the
652 indicated primary antibody overnight at 4 ℃. Reactive bands were visualised using HRP-
653 conjugated secondary antibodies and SuperSignal West Pico or Dura chemiluminescent
654 substrates (Thermo Scientific). Typically 10–20 µg total protein was loaded per lane.

655 **Real-time PCR**

656 Total RNA was extracted using TRIzol reagent (Invitrogen), followed by DNase I treatment.
657 cDNA was synthesised using the Superscript III First-Strand Synthesis System (Invitrogen)
658 with Oligo(dT) (Invitrogen). Semi-quantitative PCR was performed on 15 ng of corresponding
659 cDNA with the primers described below and utilising the SYBR Green PCR Master Mix
660 (Thermo Scientific). Relative mRNA abundance was quantified using the $2^{-\Delta\Delta CT}$ method (C_T,
661 threshold cycle), taking the housekeeping gene Tata Binding Protein (TBP) as the internal
662 control, and control siRNA-transfected cells as the calibrator (Schmittgen and Livak, 2008).
663 All PCR primers used are tabulated in **Supplementary file 1** (PCR primers for real-time PCR).

664 **Visualization of Vif-CUL5 crystal structure**

665 The previously determined structure of Vif in complex with CUL5, CBFβ, and ELOB/C (PDB
666 ID: 4N9F) was used to identify solvent-exposed residues to be mutated in this study (Guo et
667 al., 2014). Structural analysis and figures were generated using PyMOL Molecular Graphics
668 System, Version 2.0 (Schrödinger).

669 **Bioinformatic analysis of Vif polymorphisms**

Protein sequence Web Alignments for Vif, Env, Gag and Nef were downloaded from the Los Alamos HIV Sequence Alignments Database (accessible at: http://www.hiv.lanl.gov/). The following server options were selected: Alignment type, Web (all complete sequences); Organism, HIV-1/SIVcpz; Subtype, M group without recombinants (A-K); DNA/Protein, protein; Year, 2018; Format, FASTA.

These alignments contain all non-recombinant HIV-1 M group sequences from the Los Alamos HIV Sequence Database, with the following exceptions: only one sequence per patient is included; a single representative is included of very similar sequences; and sequences unlikely to represent naturally-occurring, viable viruses are excluded. We further subdivided the sequences according to viral clade (subtype) using the information in the sequence name e.g. B.FR.83.HXB2 is assigned to clade B. Analyses were conducted for both clade B viruses and all non-recombinant HIV-1 M group viruses.

To examine amino acid polymorphism in naturally occurring Vif variants at positions corresponding to residues 31, 33/34 and 128 of NL4-3 Vif, sequence logos were generated using WebLogo (Crooks et al., 2004). Further data analysis was conducted in R v.3.6.1 (R Core Team, 2019). In brief, residues at each position of interest were extracted using the seqinr R package (Charif and Lobry, 2007), then frequencies were calculated and graphical summaries generated using the ggplot R package (Wickham, 2009). To identify covariance (non-random association) between polymorphisms at positions 31 and 128, 2x2 contingency tables comparing frequencies of key residue pairs were constructed, then subjected to two-tailed Fisher's exact tests of independence (Wang and Lee, 2007).

To construct phylogenetic trees, only viruses with protein sequences available for all of Vif, Env, Gag and Nef were included. This enabled direct comparison of trees based on different viral proteins. Multiple sequence alignments and phylogenetic tree data (in Newick format) for each viral protein were generated using the Clustal Omega web server (Sievers and Higgins, 2014), then visualised using the ggtree R package (Yu et al., 2018).

All alignment and sequence files, scripts and details of the bioinformatic analyses described here are available at: https://github.com/annaprotasio/Marelli_et_al_HIV_Vif.

General statistical analysis

Where indicated, Student's *t*-tests (unpaired two-sample, assuming homoscedasticity, two-tailed), Fisher's exact tests (two-tailed) and 95% confidence intervals were calculated using Prism 7.0 (GraphPad). General data manipulation was conducted using Excel 2016 (Microsoft).

703 # Acknowledgements

704 This work was supported by the MRC (CSF MR/P008801/1 to NJM), NHSBT (WPA15-02 to
705 NJM), the Wellcome Trust (PRF 210688/Z/18/Z to PJL), the NIHR Cambridge BRC, and a
706 Wellcome Trust Strategic Award to CIMR. The authors thank Dr Reiner Schulte and the CIMR
707 Flow Cytometry Core Facility team, and members of the Matheson and Lehner laboratories
708 for critical discussion.

709

710 # Competing interests

711 The authors declare no competing interests.

Figures

Figure 1. Flow cytometric screen of HIV-1 Vif point mutants

(A) Depletion of endogenous PPP2R5D by HIV-1 Vif. CEM-T4s were transduced with transduced with lentiviruses encoding either EGFP-SBP-ΔLNGFR (Ctrl) or EGFP-P2A-Vif (Vif) at an MOI of 3, then lysed in 2% SDS and analysed by immunoblot with anti-Vif, anti-PPP2R5D and anti-β-actin (loading control) antibodies after 48 hr. Green arrows, Ctrl vs Vif.

(B) Solvent-accessible surfaces of Vif (pale blue) in complex with CUL5 (dark grey), ELOB/C (grey) and CBF-β (light grey). Residues highlighted in yellow were targeted in our library of point mutants (total 34). Residues highlighted in red specifically affected the depletion of PPP2R5B, but not APOBEC3G.

(C-D) Depletion of PPP2R5B (C) or APOBEC3G (D) by selected Vif point mutants. 293Ts stably expressing HA-tagged PPP2R5B or APOBEC3G were transfected with constructs encoding EGFP-P2A-Vif, then fixed/permeabilised, stained with AF647-conjugated anti-HA antibody and analysed by flow cytometry after 36 hr (see **Figure 1–figure supplement 1B-C**). For each Vif point mutant, abundance of PPP2R5B or APOBEC3G is shown as a ratio of A4647 fluorescence in GFP+ (transfected, Vif+) to GFP- (untransfected, Vif-) cells. Individual data points represent biological replicates (minimum 3). Mean values with standard error of the mean (SEM) are indicated. Vif point mutants specifically affecting the depletion of PPP2R5B are highlighted in red. Ctrl, control constructs encoding EGFP or EGFP-SBP-ΔLNGFR. Data for other Vif point mutants are shown in **Figure 1–figure supplement 2A-B**. Green arrows, Ctrl vs Vif WT.

(E) Representative data from (C-D). Green, GFP+, transfected cells (Vif+); grey, GFP-, untransfected cells (Vif-); dotted line, background staining of control 293Ts (no HA-tagged protein expression).

Figure 2. Depletion of endogenous APOBEC3 and PPP2R5 family proteins by HIV-1 Vif point mutants

(A) Depletion of endogenous PPP2R5D by selected Vif point mutants. CEM-T4s were transduced with lentiviruses encoding EGFP-P2A-Vif at an MOI of 3, then lysed in 2% SDS and analysed by immunoblot with anti-Vif, anti-PPP2R5D and anti-β-actin (loading control) antibodies after 48 hr. Ctrl, control construct encoding EGFP-SBP-ΔLNGFR.

(B) Overview of proteomic experiment 1 (selected Vif point mutants). CEM-T4s were transduced with lentiviruses encoding EGFP-P2A-Vif at an MOI of 3, then analysed by TMT-based quantitative proteomics after 48 hr. Mock_1/2/3, biological replicates. Ctrl, control construct encoding EGFP-SBP-ΔLNGFR.

(C-D) Depletion of endogenous PPP2R5 family (C) or APOBEC3 family (D) proteins by selected Vif point mutants in cells from (B). For each Vif point mutant, abundance of respective PPP2R5 or APOBEC family members is shown as a ratio to the mean abundance of the same family member in the 3 mock-transduced samples. Significant outliers from the distribution of abundances in mock-transduced samples are highlighted (see **Materials and methods** and **Figure 2–figure supplement 2** for further details). *p<0.05.

Figure 3. **Regulation of cell cycle by HIV-1 Vif point mutants**

(A) Phosphorylation of aurora kinases in the presence of selected Vif point mutants. CEM-T4s were transduced with lentiviruses encoding EGFP-P2A-Vif at an MOI of 3, then lysed in 2% SDS and analysed by immunoblot with anti-Vif, anti-phospho-AURK, anti-total AURKB and anti-p97 (loading control) antibodies after 48 hr. Ctrl, control construct encoding EGFP-SBP-ΔLNGFR.

(B) Regulation of cyclin B1 by selected Vif point mutants in cells from proteomic experiment 1 (**Figure 2B**). For each Vif point mutant, abundance of cyclin B1 is shown as a ratio to the

762 mean abundance in the 3 mock-transduced samples. Significant outliers from the distribution
763 of abundances in mock-transduced samples are highlighted (see **Materials and methods** for
764 details). *p<0.05; **p<0.05.

765 (C-D) Regulation of cell cycle by selected Vif point mutants. CEM-T4s were transduced with
766 lentiviruses encoding EGFP-P2A-Vif at an MOI of 3, then fixed in 90% methanol, stained with
767 7-AAD and analysed by flow cytometry after 48 hr. Representative data (C) from 3 biological
768 replicates (D) are shown. For each Vif point mutant, the fraction of cells in G2/M is shown as
769 a ratio to the fraction of cells in G2/M in mock-transduced cells. Individual data points reflect
770 biological replicates. Mean values with SEM are indicated. Significant differences compared
771 with mock-transduced cells are highlighted (*t*-tests). *p<0.05. Ctrl, control construct encoding
772 EGFP-SBP-ΔLNGFR.

773

774 **Figure 4. Regulation of cell cycle by depletion of PPP2R5 family subunits**

775 (A-B) Regulation of cell cycle by individual vs pooled PPP2R5A-E siRNA. HeLas were
776 transfected with the indicated siRNA, then fixed in 90% MeOH methanol, stained with 7-AAD
777 and analysed by flow cytometry after 48 hr. Representative data (A) from 3 biological
778 replicates (B) for each of 2 panels of siRNA are shown. For each condition, the fraction of cells
779 in G2/M is shown as a ratio to the fraction of cells in G2/M in mock-transfected cells. Individual
780 data points reflect biological replicates. Mean values with SEM are indicated. Significant
781 differences compared with mock-transduced cells are highlighted (*t*-tests). *p<0.05.
782 ***p<0.0005. Ctrl siRNA, MISSION siRNA Universal Negative Control #1. Blue
783 histograms/data points, siRNA panel 1. Red histograms/data points, siRNA panel 2.

784 (C-D) Regulation of cell cycle by combinations of pooled PPP2R5A-E siRNA. HeLas were
785 transfected with the indicated siRNA, then fixed in 90% MeOH methanol, stained with 7-AAD
786 and analysed by flow cytometry after 48 hr. Representative data (**C**) from 3 biological
787 replicates (**D**) for each of 2 panels of siRNA are shown. All details as per (**A-B**).

Figure 5. Analysis of naturally occurring HIV-1 Vif variants

(A) Amino acid polymorphism amongst 2,171 naturally occurring HIV-1 M group Vif variants (clade B). Sequence logos (left panel) and bar chart (right panel) highlight frequencies of amino acids corresponding to residues 31, 33 and 128 of NL4-3 Vif. In the sequence logos, polar amino acids (AAs) are depicted in green; neutral AAs, in purple; basic AAs, in blue; acidic AAs, in red; and hydrophobic AAs, in black. An equivalent bar chart for all naturally occurring non-recombinant HIV-1 M group Vif variants (all clades) is shown in **Figure 5–figure supplement 1**.

(B) Depletion of PPP2R5B by selected Vif point mutants. 293Ts stably expressing HA-tagged PPP2R5B were transfected with constructs encoding EGFP-P2A-Vif, then fixed/permeabilised, stained with AF647-conjugated anti-HA antibody and analysed by flow cytometry after 36 hr. Ctrl, control construct encoding EGFP-SBP-ΔLNGFR. All details as per **Figure 1B**.

(C) Sequence alignments of selected Vif variants. Amino acids corresponding to residues 31, 33 and 128 of NL4-3 Vif are highlighted in red (red boxes). Other residues targeted in our library of point mutants and known to interact with APOBEC3G (green), APOBEC3C/F (orange) and APOBEC3H (blue) are also shown (as per **Figure 1–figure supplement 2**). Additional annotations (α-helices, β-sheets, Zn finger and BC-box) are based on the published Vif-CUL5 crystal structure (Guo et al., 2014).

(D) Depletion of PPP2R5B by selected Vif variants. 293Ts stably expressing HA-tagged PPP2R5B were transfected with constructs encoding EGFP-P2A-Vif, then fixed/permeabilised, stained with AF647-conjugated anti-HA antibody and analysed by flow cytometry after 36 hr. Ctrl, control construct encoding EGFP-SBP-ΔLNGFR. All details as per (**B**) and **Figure 1B**.

Figure 6. Depletion of endogenous APOBEC3 and PPP2R5 family proteins by naturally occurring HIV-1 Vif variants

(A) Overview of proteomic experiment 2 (naturally occurring Vif variants and corresponding point mutants). CEM-T4s were transduced with lentiviruses encoding EGFP-P2A-Vif at an MOI of 3, then analysed by TMT-based quantitative proteomics after 48 hr. Mock_1/2/3, biological replicates. Ctrl, control construct encoding EGFP. NL4-3 AYR, NL4-3 Vif with both I31A and RI127/128YR mutations.

(B-C) Depletion of endogenous PPP2R5 family (B) or APOBEC3 family (C) proteins by naturally occurring Vif variants and corresponding point mutants in cells from (A). For each Vif variant or point mutant, abundance of respective PPP2R5 or APOBEC family members is shown as a ratio to the mean abundance of the same family member in the 3 mock-transduced samples. Significant outliers from the distribution of abundances in mock-transduced samples are highlighted (see **Materials and methods** and **Figure 2–figure supplement 2** for further details). *p<0.05; **p<0.005. † Not detected in this experiment (PPP2R5B, APOBEC3F).

(D) Regulation of cell cycle by naturally occurring Vif variants and corresponding point mutants. CEM-T4s were transduced with lentiviruses encoding EGFP-P2A-Vif at an MOI of 3, then fixed in 90% methanol, stained with 7-AAD and analysed by flow cytometry after 48 hr. Individual data points reflect 3 biological replicates (representative data, **Figure 6–figure supplement 3**). **p<0.005. ***p<0.0005. Ctrl, control construct encoding EGFP. NL4-3 AYR, NL4-3 Vif with both I31A and RI127/128YR mutations. All other details as per **Figure 3C-D**.

Figure 7. Selective regulation of PPP2R5 family subunits during HIV-1 infection

(A) Overview of proteomic experiment 3 (viral infections). CEM-T4s were infected with HIV-AFMACS viruses at an MOI of 0.5, then purified using AFMACS (**Figure 7–figure supplement 1A-B**) and analysed by TMT-based quantitative proteomics after 48 hr. Biological replicates are shown. Vif AYR, NL4-3 Vif with both I31A and RI127/128YR mutations.

(B) Protein abundances in HIV-infected vs mock-infected cells from (A). Volcano plots show statistical significance (*y*-axis) vs fold change (*x*-axis) for 6,294 viral and cellular proteins (no missing values). Pair-wise comparisons of mock-infected cells with cells infected with ΔVpr-Vif WT (left panel), ΔVpr-ΔVif (middle panel) or ΔVpr-Vif AYR (right panel) viruses are shown. Proteins with Benjamini-Hochberg FDR-adjusted p values (q values) <0.05 (black crosses) or >0.05 (grey crosses) are indicated (FDR threshold of 5%). Proteins highlighted in each plot are summarised in the key. 4 out of 5 PPP2R5 family subunits (A/C/D/E) were quantitated, but only 1 out of 7 APOBEC3 family member (C).

(C) Regulation of cell cycle in HIV-infected cells. CEM-T4s were infected with HIV-AFMACS viruses at an MOI of 0.5, then stained with FITC-conjugated anti-LNGFR antibody, fixed in 90% methanol, stained with 7-AAD and analysed by flow cytometry after 48 hr. Representative data (upper panels) from 3 biological replicates (lower panel) are shown. Green, LNGFR+ cells (HIV+); grey, LNGFR- cells (uninfected). For each virus, the fraction of HIV+ (LNGFR+) cells in G2/M is shown as a ratio to the fraction of cells in G2/M in uninfected (LNGFR-) cells. Individual data points reflect biological replicates. Mean values with SEM are indicated. Significant differences are highlighted for each pair-wise comparison (*t*-tests). **p<0.005.

(D) Pair-wise combinations of key amino acid polymorphisms amongst 2,171 naturally occurring HIV-1 M group Vif variants (clade B). Frequencies of amino acids corresponding to residues 31 and 128 of NL4-3 Vif are shown. An equivalent pie chart for all naturally occurring non-recombinant HIV-1 M group Vif variants (all clades) is shown in **Figure 7–figure supplement 2B**.

(E) Phylogenetic tree of 795 HIV-1 M group viruses (clade B) with protein sequences available for all of Vif, Gag, Env and Nef (based on relatedness of Vif). Viruses encoding Vif variants with I31/I128 (most active, red) and V31/R128 (least active, blue) are highlighted. Equivalent phylogenetic trees based on relatedness of Gag, Env or Nef are shown in **Figure 7–figure supplement 3A**.

Figure supplements

Figure 1–figure supplement 1. Further details for site-directed mutagenesis and flow cytometric screen

(A) Overview of PCR and Gibson assembly-based approach to site-directed mutagenesis. PCR products are digested with DpnI (1 hr, 37 °C) to degrade template. Vector is digested with XhoI and KpnI, gel purified, then assembled with PCR products using the NEBuilder HiFi DNA Assembly Master Mix (1 hr, 50 °C) and transformed into competent cells. Mut_Fwd and Mut_Rvs, mutation-specific primers; Vif_Fwd and Vif_Rvs, common primers; seq, sequencing primer; red circle, site of intended mutation; red cross, intended mutation; red parallel lines, cut sites; orange boxes, overlapping sequences.

(B) Overview of flow cytometeric screen. 293Ts stably expressing HA-tagged PPP2R5B or APOBEC3G were transfected with constructs encoding EGFP-P2A-Vif, then fixed/permeabilised, stained with AF647-conjugated anti-HA antibody and analysed by flow cytometry after 36 hr.

(C) Illustrative data and gating strategy for flow cytometric screen. A4647 fluorescence indicates abundance of PPP2R5B. For each Vif point mutant, A4647 fluorescence is compared between Green, GFP+, transfected cells (Vif+); grey, GFP-, untransfected cells (Vif-); dotted line, background staining of control 293Ts (no HA-tagged protein expression). Upper panels, control construct encoding EGFP; lower panels, construct encoding EGFP-P2A-Vif (WT).

Figure 1–figure supplement 2. Complete results of flow cytometric screen

(A-B) Depletion of PPP2R5B (A) or APOBEC3G (B) by all Vif point mutants targeted in our library. 293Ts stably expressing HA-tagged PPP2R5B or APOBEC3G were transfected with constructs encoding EGFP-P2A-Vif, then fixed/permeabilised, stained with AF647-conjugated anti-HA antibody and analysed by flow cytometry after 36 hr (see **Figure 1–figure**

892 **supplement 1B-C**). For each Vif point mutant, abundance of PPP2R5B or APOBEC3G is
893 shown as a ratio of A4647 fluorescence in GFP+ (transfected, Vif+) to GFP- (untransfected,
894 Vif-) cells. Individual data points represent biological replicates (minimum 2). Mean values with
895 SEM are indicated. Vif point mutants specifically affecting the depletion of PPP2R5B are
896 highlighted in red (also shown in **Figure 1B-D**). Other residues included in our screen and
897 known to interact with APOBEC3G (green), APOBEC3C/F (orange) and APOBEC3H (blue)
898 are also indicated (Gaddis et al., 2003; Letko et al., 2015; Nakashima et al., 2016; Ooms et
899 al., 2016). Ctrl, control construct encoding EGFP or EGFP-SBP-ΔLNGFR.

900 (C) Solvent-accessible surfaces of Vif (pale blue) in complex with CUL5 (dark grey), ELOB/C
901 (grey) and CBF-β (light grey). Residues specifically affecting the depletion of PPP2R5B are
902 highlighted in red, together with residues included in our screen and known to interact with
903 APOBEC3G (green), APOBEC3C/F (orange) and APOBEC3H (blue), as per (A-B).

904

905 **Figure 2–figure supplement 1. Stability of selected Vif point mutants**

906 Expression of selected Vif point mutants in cells from proteomic experiment 1 (**Figure 2B**).
907 For each Vif point mutant, abundance is shown as a ratio to Vif WT.

908

909 **Figure 2–figure supplement 2. Calculation of *t*-scores and *p*-values**

910 Illustrative *t*-score/*p*-value calculations for PPP2R5A in cells transduced with EGFP-SBP-
911 ΔLNGFR (control lentivector) or WT Vif. Graphs show protein abundance (x axis) vs probability
912 density (y axis). A *t*-distribution (2 degrees of freedom) based on PPP2R5A abundances in
913 mock-transduced cells (3 biological replicates) is shown (grey bell curve). Abundances from
914 mock-transduced cells (grey data points, all panels), cells transduced with EGFP-SBP-
915 ΔLNGFR (Ctrl, blue data point, middle panel) or Vif WT (red data point, right panel) are
916 projected on to the distribution for illustrative purposes. Standard scores (*t*-scores) indicate

distance (number of standards deviations, *S*) from the sample mean ($\overline{x}$). Corresponding two-tailed *p*-values are shown. Note that for a *t*-distribution with 2 degrees of freedom, the 95% confidence interval lies within +/- 4.30 standard deviations of the mean, compared with +/- 1.96 standard deviations of the mean for the normal distribution (*z*-distribution).

Figure 3–figure supplement 1. Additional controls for cell cycle analysis (Vif point mutants)

(A-B) Regulation of cell cycle by selected Vif point mutants. CEM-T4s were transduced with lentiviruses encoding EGFP-P2A-Vif at an MOI of 3, then fixed in 90% methanol, stained with 7-AAD and analysed by flow cytometry after 48 hr. Representative data (A) from 2 biological replicates (B) are shown. Mean values are indicated. Ctrl, control construct encoding EGFP-SBP-ΔLNGFR. All other details as per **Figure 3C-D**.

Figure 3–figure supplement 2. Depletion of endogenous DPH7 and FMR1 by selected Vif point mutants

(A) Depletion of DPH7 (left panel) and FMR1 (right panel) by selected Vif point mutants in cells from proteomic experiment 1 (**Figure 2B**). For each Vif point mutant, abundances of DPH7 and FMR1 are shown as a ratio to the mean abundances in the 3 mock-transduced samples. Significant outliers from the distribution of abundances in mock-transduced samples are highlighted (see **Materials and methods** for details). *p<0.05.

Figure 4–figure supplement 1. Additional controls for cell cycle analysis (PPP2R5A-E siRNA)

(A) Regulation of cell cycle by PP2A inhibition. CEM-T4s were treated with either 100nM Okadaic acid or DMSO (vehicle) for 16 hr, then fixed in 90% methanol, stained with 7-AAD and analysed by flow cytometry.

(B) Regulation of cell cycle in HeLas by Vif. Cells were transduced with GFP-P2A-Vif at an MOI of 3, then fixed in 90% methanol, stained with 7-AAD and analysed by flow cytometry after 48 hr. Ctrl, control construct encoding EGFP.

(C) Efficiency of PPP2R5A-E knockdown. HeLas were transfected with pooled PPP2R5A-E siRNAs (as per **Figure 4**), then analysed by real-time PCR after 24 hr. For each PPP2R5 family subunit, relative mRNA abundance is shown as a ratio to the abundance in control siRNA-transfected cells (Ctrl), normalized to Tata Binding Protein (TBP) expression. Individual data points represent 2 biological replicates for each of 2 panels of siRNA. Mean values are indicated.

Figure 4–figure supplement 2. Additional controls for cell cycle analysis (DPH7 and FMR1 siRNA)

(A-B) Regulation of cell cycle by DPH7 and FMR1 siRNA. HeLas were transfected with the indicated siRNA, then fixed in 90% MeOH methanol, stained with 7-AAD and analysed by flow cytometry after 48 hr. Representative data (A) from 3 biological replicates (B) for each of 2 siRNAs are shown. For each condition, the fraction of cells in G2/M is shown as a ratio to the fraction of cells in G2/M in mock-transfected cells. Individual data points reflect biological replicates. Mean values with 95% confidence intervals (CIs) are indicated. Ctrl siRNA, MISSION siRNA Universal Negative Control #1.

(C) Efficiency of DPH7 and FMR1 knockdown. Cells from (A-B) were lysed in 2% SDS 24 hr after siRNA transfection and analysed by immunoblot with anti-FMR, anti-DPH7 and anti-β-actin (loading control) antibodies.

Figure 5–figure supplement 1.

Amino acid polymorphism amongst 3,412 naturally occurring non-recombinant HIV-1 M group Vif variants (all clades). Bar chart highlights frequencies of amino acids corresponding to residues 31, 33 and 128 of NL4-3 Vif.

Figure 5–figure supplement 2. Depletion of APOBEC3G by selected Vif variants

Depletion of APOBEC3G by selected Vif variants. 293Ts stably expressing HA-tagged APOBEC3G were transfected with constructs encoding EGFP-P2A-Vif, then fixed/permeabilised, stained with AF647-conjugated anti-HA antibody and analysed by flow cytometry after 36 hr. Ctrl, control construct encoding EGFP-SBP-ΔLNGFR. All details as per **Figure 1B**.

Figure 6–figure supplement 1. Sequence of Exonic Splicing Silencer of Vpr (ESSV) in NL4-3 and YU2 Vif variants

The ESSV (highlighted in bold) is a short nucleotide element within the HIV-1 Vif open reading frame (exon 3) required to repress splicing at HIV-1 3' splice site A2 and allow accumulation of unspliced mRNA, production of Gag and HIV viral replication (Madsen and Stoltzfus, 2005). Inhibitory activity is dependent on three (Py/A)UAG motifs (indicated with black lines). Introduction of an isolated I128R mutation into NL4-3 Vif would disrupt the second (Py/A)UAG motif. Conversely, simultaneous introduction of an R127Y mutation (as in YU2 Vif) maintains three (Py/A)UAG motifs. Note that the nucleotide (nucl) and amino acid (aa) sequences flanking these positions is otherwise conserved between NL4-3 and YU2 viruses.

Figure 6–figure supplement 2. Depletion of PPP2R5B and APOBEC3G by Vif AYR

(A-B) 293Ts stably expressing HA-tagged PPP2R5B or APOBEC3G were transfected with constructs encoding EGFP-P2A-Vif, then fixed/permeabilised, stained with AF647-conjugated anti-HA antibody and analysed by flow cytometry after 36 hr. Representative data (A) from 3 biological replicates (B) are shown. Ctrl, control construct encoding EGFP. All details as per **Figure 1B**.

Figure 6–figure supplement 3. Regulation of cell cycle by naturally occurring Vif variants and corresponding point mutants (representative data)

CEM-T4s were transduced with lentiviruses encoding EGFP-P2A-Vif at an MOI of 3, then fixed in 90% methanol, stained with 7-AAD and analysed by flow cytometry after 48 hr. Representative data from **Figure 6D**.

Figure 7–figure supplement 1. AFMACS-based purification of infected cells for proteomic experiment 3 (viral infections)

HIV-infected cells from **Figure 7A** were stained with anti-LNGFR and anti-CD4 antibodies and analysed by flow cytometry before (input) and after (purified vs flow-through) selection using AFMACS. Purified cells were used for proteomic analysis. Infected cells express the SBP-ΔLNGFR cell surface affinity tag (LNGFR+) and downregulate CD4 through the action of Nef and Vpu (Guy et al., 1987; Naamati et al., 2019; Willey et al., 1992). Representative data (A) from 3 biological replicates (B) are shown. Vif AYR, NL4-3 Vif with both I31A and RI127/128YR mutations.

Figure 7–figure supplement 2. Additional bioinformatics analysis

(A) Contingency tables showing combinations of key amino acid polymorphisms amongst naturally occurring HIV-1 M group Vif variants (clade B) summarised in **Figure 7D**.

(B) Pair-wise combinations of key amino acid polymorphisms amongst 3,412 naturally occurring non-recombinant HIV-1 M group Vif variants (all clades). Frequencies of amino acids corresponding to residues 31 and 128 of NL4-3 Vif are shown. Same sequences as **Figure 5–figure supplement 1**.

(C) Contingency tables showing combinations of key amino acid polymorphisms amongst naturally occurring non-recombinant HIV-1 M group Vif variants (all clades) summarised in (B).

Figure 7–figure supplement 2. Additional phylogenetic trees

(A) Phylogenetic trees of 795 HIV-1 M group viruses (clade B) with protein sequences available for all of Vif, Gag, Env and Nef (based on relatedness of Gag, Env or Nef). Viruses encoding Vif variants with I31/I128 (most active, red) and V31/R128 (least active, blue) are highlighted.

(B) Phylogenetic trees of 1,649 naturally occurring non-recombinant HIV-1 M group viruses (all clades) with protein sequences available for all of Vif, Gag, Env and Nef (based on relatedness of Vif). In the left panel, viruses encoding Vif variants with I31/I128 (most active, red) and V31/R128 (least active, blue) are highlighted. In the right panel (same phylogenetic tree), viruses are coloured according to clade (as indicated).

Source data

Figure 2–source data 1. Complete data from proteomic experiment 1 (selected Vif point mutants)

Complete dataset (unfiltered) from TMT-based quantitative proteomic experiment illustrated in **Figure 2B**. For each protein, normalised, unscaled protein abundances, the number of unique peptides used for protein quantitation, and the protein FDR confidence are shown.

Figure 6–source data 1. Complete data from proteomic experiment 2 (naturally occurring Vif variants and corresponding point mutants)

Complete dataset (unfiltered) from TMT-based quantitative proteomic experiment illustrated in **Figure 6A**. For each protein, normalised, unscaled protein abundances, the number of unique peptides used for protein quantitation, and the protein FDR confidence are shown.

Figure 7–source data 1. Complete data from proteomic experiment 3 (viral infections)

Complete dataset (unfiltered) from TMT-based quantitative proteomic experiment illustrated in **Figure 7A**. For each protein, normalised, unscaled protein abundances, the number of unique peptides used for protein quantitation, and the protein FDR confidence are shown.

Supplementary files

Supplementary file 1. DNA and RNA sequences

Sequences of PCR primers for Vif mutant library construction, codon-optimised Vif variants synthesised as gBlocks, Vif YRA in pNL4-3-dEnv-Nef-P2A-SBP-ΔLNGFR, oligonucleotides for RNAi and primers for real-time PCR.

References

Ajay, A.K., Upadhyay, A.K., Singh, S., Vijayakumar, M.V., Kumari, R., Pandey, V., Boppana, R., and Bhat, M.K. (2010). Cdk5 phosphorylates non-genotoxically overexpressed p53 following inhibition of PP2A to induce cell cycle arrest/apoptosis and inhibits tumor progression. Mol Cancer *9*, 204.

Bagga, S., and Bouchard, M.J. (2014). Cell cycle regulation during viral infection. Methods Mol Biol *1170*, 165-227.

Berger, G., Durand, S., Fargier, G., Nguyen, X.N., Cordeil, S., Bouaziz, S., Muriaux, D., Darlix, J.L., and Cimarelli, A. (2011). APOBEC3A is a specific inhibitor of the early phases of HIV-1 infection in myeloid cells. PLoS Pathog *7*, e1002221.

Binka, M., Ooms, M., Steward, M., and Simon, V. (2012a). The Activity Spectrum of Vif from Multiple HIV-1 Subtypes against APOBEC3G, APOBEC3F, and APOBEC3H. *86*, 49-59.

Binka, M., Ooms, M., Steward, M., and Simon, V. (2012b). The activity spectrum of Vif from multiple HIV-1 subtypes against APOBEC3G, APOBEC3F, and APOBEC3H. J Virol *86*, 49-59.

Charif, D., and Lobry, J.R. (2007). Seqin{R} 1.0-2: a contributed package to the {R} project for statistical computing devoted to biological sequences retrieval and analysis. In Structural approaches to sequence evolution: Molecules, networks, populations, U. Bastolla, M. Porto, R.H. E., and M. Vendruscolo, eds. (New York: Springer Verlag), pp. 207-232.

Chen, G., He, Z., Wang, T., Xu, R., and Yu, X.F. (2009). A Patch of Positively Charged Amino Acids Surrounding the Human Immunodeficiency Virus Type 1 Vif SLVx4Yx9Y Motif Influences Its Interaction with APOBEC3G. J Virol *83*, 8674-8682.

Compton, A.A., Malik, H.S., and Emerman, M. (2013). Host gene evolution traces the evolutionary history of ancient primate lentiviruses. Philos Trans R Soc Lond B Biol Sci *368*, 20120496.

1080 Conticello, S.G., Harris, R.S., and Neuberger, M.S. (2003). The Vif protein of HIV triggers
1081 degradation of the human antiretroviral DNA deaminase APOBEC3G. Curr Biol *13*, 2009-
1082 2013.
1083 Crooks, G.E., Hon, G., Chandonia, J.M., and Brenner, S.E. (2004). WebLogo: a sequence
1084 logo generator. Genome Res *14*, 1188-1190.
1085 Dang, Y., Wang, X., Zhou, T., York, I.A., and Zheng, Y.H. (2009). Identification of a Novel
1086 WxSLVK Motif in the N Terminus of Human Immunodeficiency Virus and Simian
1087 Immunodeficiency Virus Vif That Is Critical for APOBEC3G and APOBEC3F Neutralization. J
1088 Virol *83*, 8544-8552.
1089 DeHart, J.L., Bosque, A., Harris, R.S., and Planelles, V. (2008). Human immunodeficiency
1090 virus type 1 Vif induces cell cycle delay via recruitment of the same E3 ubiquitin ligase
1091 complex that targets APOBEC3 proteins for degradation. J Virol *82*, 9265-9272.
1092 Doehle, B.P., Schafer, A., and Cullen, B.R. (2005). Human APOBEC3B is a potent inhibitor
1093 of HIV-1 infectivity and is resistant to HIV-1 Vif. Virology *339*, 281-288.
1094 Evans, E.L., 3rd, Becker, J.T., Fricke, S.L., Patel, K., and Sherer, N.M. (2018). HIV-1 Vif's
1095 Capacity To Manipulate the Cell Cycle Is Species Specific. J Virol *92*.
1096 Fenton-May, A.E., Dibben, O., Emmerich, T., Ding, H., Pfafferott, K., Aasa-Chapman, M.M.,
1097 Pellegrino, P., Williams, I., Cohen, M.S., Gao, F.*, et al.* (2013). Relative resistance of HIV-1
1098 founder viruses to control by interferon-alpha. Retrovirology *10*, 146.
1099 Foley, E.A., Maldonado, M., and Kapoor, T.M. (2011). Formation of stable attachments
1100 between kinetochores and microtubules depends on the B56-PP2A phosphatase. Nature
1101 cell biology *13*, 1265-1271.
1102 Foley, G.E., Handler, A.H., Lynch, P.M., Wolman, S.R., Stulberg, C.S., and Eagle, H. (1965).
1103 Loss of neoplastic properties in vitro. II. Observations on KB sublines. Cancer Res *25*, 1254-
1104 1261.
1105 Gabuzda, D.H., Lawrence, K., Langhoff, E., Terwilliger, E., Dorfman, T., Haseltine, W.A.,
1106 and Sodroski, J. (1992). Role of vif in replication of human immunodeficiency virus type 1 in
1107 CD4+ T lymphocytes. J Virol *66*, 6489-6495.

1108 Gaddis, N.C., Chertova, E., Sheehy, A.M., Henderson, L.E., and Malim, M.H. (2003).
1109 Comprehensive investigation of the molecular defect in vif-deficient human
1110 immunodeficiency virus type 1 virions. J Virol *77*, 5810-5820.
1111 Geiger, T., Wehner, A., Schaab, C., Cox, J., and Mann, M. (2012). Comparative proteomic
1112 analysis of eleven common cell lines reveals ubiquitous but varying expression of most
1113 proteins. Mol Cell Proteomics *11*, M111 014050.
1114 Goh, W.C., Rogel, M.E., Kinsey, C.M., Michael, S.F., Fultz, P.N., Nowak, M.A., Hahn, B.H.,
1115 and Emerman, M. (1998). HIV-1 Vpr increases viral expression by manipulation of the cell
1116 cycle: a mechanism for selection of Vpr in vivo. Nat Med *4*, 65-71.
1117 Grallert, A., Boke, E., Hagting, A., Hodgson, B., Connolly, Y., Griffiths, J.R., Smith, D.L.,
1118 Pines, J., and Hagan, I.M. (2015). A PP1-PP2A phosphatase relay controls mitotic
1119 progression. Nature *517*, 94-98.
1120 Greenwood, E.J., Matheson, N.J., Wals, K., van den Boomen, D.J., Antrobus, R.,
1121 Williamson, J.C., and Lehner, P.J. (2016). Temporal proteomic analysis of HIV infection
1122 reveals remodelling of the host phosphoproteome by lentiviral Vif variants. Elife *5*.
1123 Greenwood, E.J.D., Williamson, J.C., Sienkiewicz, A., Naamati, A., Matheson, N.J., and
1124 Lehner, P.J. (2019). Promiscuous Targeting of Cellular Proteins by Vpr Drives Systems-
1125 Level Proteomic Remodeling in HIV-1 Infection. Cell Rep *27*, 1579-1596 e1577.
1126 Gummuluru, S., and Emerman, M. (1999). Cell cycle- and Vpr-mediated regulation of human
1127 immunodeficiency virus type 1 expression in primary and transformed T-cell lines. J Virol *73*,
1128 5422-5430.
1129 Guo, Y., Dong, L., Qiu, X., Wang, Y., Zhang, B., Liu, H., Yu, Y., Zang, Y., Yang, M., and
1130 Huang, Z. (2014). Structural basis for hijacking CBF-beta and CUL5 E3 ligase complex by
1131 HIV-1 Vif. Nature *505*, 229-233.
1132 Guy, B., Kieny, M.P., Riviere, Y., Le Peuch, C., Dott, K., Girard, M., Montagnier, L., and
1133 Lecocq, J.P. (1987). HIV F/3' orf encodes a phosphorylated GTP-binding protein resembling
1134 an oncogene product. Nature *330*, 266-269.

Harris, R.S., and Anderson, B.D. (2016). Evolutionary Paradigms from Ancient and Ongoing Conflicts between the Lentiviral Vif Protein and Mammalian APOBEC3 Enzymes. PLOS Pathogens *12*, e1005958.

He, J., Choe, S., Walker, R., Di Marzio, P., Morgan, D.O., and Landau, N.R. (1995). Human immunodeficiency virus type 1 viral protein R (Vpr) arrests cells in the G2 phase of the cell cycle by inhibiting p34cdc2 activity. J Virol *69*, 6705-6711.

He, Z., Zhang, W., Chen, G., Xu, R., and Yu, X.-F. (2008). Characterization of Conserved Motifs in HIV-1 Vif Required for APOBEC3G and APOBEC3F Interaction. *381*, 1000-1011.

Hertz, E.P.T., Kruse, T., Davey, N.E., Lopez-Mendez, B., Sigurethsson, J.O., Montoya, G., Olsen, J.V., and Nilsson, J. (2016). A Conserved Motif Provides Binding Specificity to the PP2A-B56 Phosphatase. Mol Cell *63*, 686-695.

Hultquist, J.F., Lengyel, J.A., Refsland, E.W., LaRue, R.S., Lackey, L., Brown, W.L., and Harris, R.S. (2011). Human and rhesus APOBEC3D, APOBEC3F, APOBEC3G, and APOBEC3H demonstrate a conserved capacity to restrict Vif-deficient HIV-1. J Virol *85*, 11220-11234.

Iwabu, Y., Kinomoto, M., Tatsumi, M., Fujita, H., Shimura, M., Tanaka, Y., Ishizaka, Y., Nolan, D., Mallal, S., Sata, T.*, et al.* (2010). Differential anti-APOBEC3G activity of HIV-1 Vif proteins derived from different subtypes. J Biol Chem *285*, 35350-35358.

Izumi, T., Io, K., Matsui, M., Shirakawa, K., Shinohara, M., Nagai, Y., Kawahara, M., Kobayashi, M., Kondoh, H., Misawa, N.*, et al.* (2010). HIV-1 viral infectivity factor interacts with TP53 to induce G2 cell cycle arrest and positively regulate viral replication. Proc Natl Acad Sci U S A *107*, 20798-20803.

Jowett, J.B., Planelles, V., Poon, B., Shah, N.P., Chen, M.L., and Chen, I.S. (1995). The human immunodeficiency virus type 1 vpr gene arrests infected T cells in the G2 + M phase of the cell cycle. J Virol *69*, 6304-6313.

Kobayashi, M., Takaori-Kondo, A., Miyauchi, Y., Iwai, K., and Uchiyama, T. (2005). Ubiquitination of APOBEC3G by an HIV-1 Vif-Cullin5-Elongin B-Elongin C complex is essential for Vif function. J Biol Chem *280*, 18573-18578.

1163 Koning, F.A., Newman, E.N., Kim, E.Y., Kunstman, K.J., Wolinsky, S.M., and Malim, M.H.
1164 (2009). Defining APOBEC3 expression patterns in human tissues and hematopoietic cell
1165 subsets. J Virol *83*, 9474-9485.
1166 Laguette, N., Bregnard, C., Hue, P., Basbous, J., Yatim, A., Larroque, M., Kirchhoff, F.,
1167 Constantinou, A., Sobhian, B., and Benkirane, M. (2014). Premature activation of the SLX4
1168 complex by Vpr promotes G2/M arrest and escape from innate immune sensing. Cell *156*,
1169 134-145.
1170 Lee, S.J., Rodriguez-Bravo, V., Kim, H., Datta, S., and Foley, E.A. (2017). The PP2A(B56)
1171 phosphatase promotes the association of Cdc20 with APC/C in mitosis. J Cell Sci *130*, 1760-
1172 1771.
1173 Letko, M., Booiman, T., Kootstra, N., Simon, V., and Ooms, M. (2015). Identification of the
1174 HIV-1 Vif and Human APOBEC3G Protein Interface. Cell Reports *13*, 1789-1799.
1175 Li, X., Scuderi, A., Letsou, A., and Virshup, D.M. (2002). B56-associated protein
1176 phosphatase 2A is required for survival and protects from apoptosis in Drosophila
1177 melanogaster. Mol Cell Biol *22*, 3674-3684.
1178 Liu, M.K., Hawkins, N., Ritchie, A.J., Ganusov, V.V., Whale, V., Brackenridge, S., Li, H.,
1179 Pavlicek, J.W., Cai, F., Rose-Abrahams, M.*, et al.* (2013). Vertical T cell immunodominance
1180 and epitope entropy determine HIV-1 escape. J Clin Invest *123*, 380-393.
1181 Madsen, J.M., and Stoltzfus, C.M. (2005). An exonic splicing silencer downstream of the 3'
1182 splice site A2 is required for efficient human immunodeficiency virus type 1 replication. J
1183 Virol *79*, 10478-10486.
1184 Marin, M., Rose, K.M., Kozak, S.L., and Kabat, D. (2003). HIV-1 Vif protein binds the editing
1185 enzyme APOBEC3G and induces its degradation. Nat Med *9*, 1398-1403.
1186 Matheson, N.J., Peden, A.A., and Lehner, P.J. (2014). Antibody-free magnetic cell sorting of
1187 genetically modified primary human CD4+ T cells by one-step streptavidin affinity
1188 purification. PLoS One *9*, e111437.
1189 Matheson, N.J., Sumner, J., Wals, K., Rapiteanu, R., Weekes, M.P., Vigan, R., Weinelt, J.,
1190 Schindler, M., Antrobus, R., Costa, A.S.*, et al.* (2015). Cell Surface Proteomic Map of HIV

Infection Reveals Antagonism of Amino Acid Metabolism by Vpu and Nef. Cell Host Microbe *18*, 409-423.

Mehle, A., Strack, B., Ancuta, P., Zhang, C., McPike, M., and Gabuzda, D. (2004). Vif overcomes the innate antiviral activity of APOBEC3G by promoting its degradation in the ubiquitin-proteasome pathway. J Biol Chem *279*, 7792-7798.

Mehle, A., Wilson, H., Zhang, C., Brazier, A.J., McPike, M., Pery, E., and Gabuzda, D. (2007). Identification of an APOBEC3G Binding Site in Human Immunodeficiency Virus Type 1 Vif and Inhibitors of Vif-APOBEC3G Binding. J Virol *81*, 13235-13241.

Menzies, S.A., Volkmar, N., van den Boomen, D.J., Timms, R.T., Dickson, A.S., Nathan, J.A., and Lehner, P.J. (2018). The sterol-responsive RNF145 E3 ubiquitin ligase mediates the degradation of HMG-CoA reductase together with gp78 and Hrd1. Elife *7*.

Miles, A.L., Burr, S.P., Grice, G.L., and Nathan, J.A. (2017). The vacuolar-ATPase complex and assembly factors, TMEM199 and CCDC115, control HIF1alpha prolyl hydroxylation by regulating cellular iron levels. Elife *6*.

Mulder, L.C., Harari, A., and Simon, V. (2008). Cytidine deamination induced HIV-1 drug resistance. Proc Natl Acad Sci U S A *105*, 5501-5506.

Naamati, A., Williamson, J.C., Greenwood, E.J., Marelli, S., Lehner, P.J., and Matheson, N.J. (2019). Functional proteomic atlas of HIV infection in primary human CD4+ T cells. Elife *8*.

Nakano, Y., Aso, H., Soper, A., Yamada, E., Moriwaki, M., Juarez-Fernandez, G., Koyanagi, Y., and Sato, K. (2017). A conflict of interest: the evolutionary arms race between mammalian APOBEC3 and lentiviral Vif. Retrovirology *14*, 31.

Nakashima, M., Ode, H., Kawamura, T., Kitamura, S., Naganawa, Y., Awazu, H., Tsuzuki, S., Matsuoka, K., Nemoto, M., Hachiya, A.*, et al.* (2016). Structural Insights into HIV-1 Vif-APOBEC3F Interaction. *90*, 1034-1047.

Nasa, I., and Kettenbach, A.N. (2018). Coordination of Protein Kinase and Phosphoprotein Phosphatase Activities in Mitosis. Front Cell Dev Biol *6*, 30.

Ooms, M., Letko, M., and Simon, V. (2016). The structural interface between HIV-1 Vif and human APOBEC3H. JVI.02289-02216.

Parrish, N.F., Gao, F., Li, H., Giorgi, E.E., Barbian, H.J., Parrish, E.H., Zajic, L., Iyer, S.S., Decker, J.M., Kumar, A.*, et al.* (2013). Phenotypic properties of transmitted founder HIV-1. Proc Natl Acad Sci U S A *110*, 6626-6633.

Peng, G., Greenwell-Wild, T., Nares, S., Jin, W., Lei, K.J., Rangel, Z.G., Munson, P.J., and Wahl, S.M. (2007). Myeloid differentiation and susceptibility to HIV-1 are linked to APOBEC3 expression. Blood *110*, 393-400.

R Core Team (2019). R: A language and environment for statistical computing (Vienna, Austria: R Foundation for Statistical Computing).

Refsland, E.W., Stenglein, M.D., Shindo, K., Albin, J.S., Brown, W.L., and Harris, R.S. (2010). Quantitative profiling of the full APOBEC3 mRNA repertoire in lymphocytes and tissues: implications for HIV-1 restriction. Nucleic Acids Res *38*, 4274-4284.

Richards, C., John, Demir, Ö., Nadine, Elizabeth, Allison, Brett, John, John, Daniel*, et al.* (2015). The Binding Interface between Human APOBEC3F and HIV-1 Vif Elucidated by Genetic and Computational Approaches. Cell Reports *13*, 1781-1788.

Ritchie, M.E., Phipson, B., Wu, D., Hu, Y., Law, C.W., Shi, W., and Smyth, G.K. (2015). limma powers differential expression analyses for RNA-sequencing and microarray studies. Nucleic Acids Res *43*, e47.

Rogel, M.E., Wu, L.I., and Emerman, M. (1995). The human immunodeficiency virus type 1 vpr gene prevents cell proliferation during chronic infection. J Virol *69*, 882-888.

Russell, R.A., and Pathak, V.K. (2007). Identification of Two Distinct Human Immunodeficiency Virus Type 1 Vif Determinants Critical for Interactions with Human APOBEC3G and APOBEC3F. J Virol *81*, 8201-8210.

Sakai, K., Dimas, J., and Lenardo, M.J. (2006). The Vif and Vpr accessory proteins independently cause HIV-1-induced T cell cytopathicity and cell cycle arrest. Proc Natl Acad Sci U S A *103*, 3369-3374.

1245 Schmittgen, T.D., and Livak, K.J. (2008). Analyzing real-time PCR data by the comparative
1246 C(T) method. Nat Protoc *3*, 1101-1108.
1247 Schwammle, V., Leon, I.R., and Jensen, O.N. (2013). Assessment and improvement of
1248 statistical tools for comparative proteomics analysis of sparse data sets with few
1249 experimental replicates. J Proteome Res *12*, 3874-3883.
1250 Sheehy, A.M., Gaddis, N.C., Choi, J.D., and Malim, M.H. (2002). Isolation of a human gene
1251 that inhibits HIV-1 infection and is suppressed by the viral Vif protein. Nature *418*, 646-650.
1252 Sheehy, A.M., Gaddis, N.C., and Malim, M.H. (2003). The antiretroviral enzyme APOBEC3G
1253 is degraded by the proteasome in response to HIV-1 Vif. Nat Med *9*, 1404-1407.
1254 Sievers, F., and Higgins, D.G. (2014). Clustal Omega, accurate alignment of very large
1255 numbers of sequences. Methods Mol Biol *1079*, 105-116.
1256 Simon, J.H., Southerling, T.E., Peterson, J.C., Meyer, B.E., and Malim, M.H. (1995).
1257 Complementation of vif-defective human immunodeficiency virus type 1 by primate, but not
1258 nonprimate, lentivirus vif genes. J Virol *69*, 4166-4172.
1259 Simon, V., Zennou, V., Murray, D., Huang, Y., Ho, D.D., and Bieniasz, P.D. (2005a). Natural
1260 variation in Vif: differential impact on APOBEC3G/3F and a potential role in HIV-1
1261 diversification. PLoS Pathog *1*, e6.
1262 Simon, V., Zennou, V., Murray, D., Huang, Y., Ho, D.D., and Bieniasz, P.D. (2005b). Natural
1263 Variation in Vif: Differential Impact on APOBEC3G/3F and a Potential Role in HIV-1
1264 Diversification. PLoS Pathogens *1*, e6.
1265 Stopak, K., de Noronha, C., Yonemoto, W., and Greene, W.C. (2003). HIV-1 Vif blocks the
1266 antiviral activity of APOBEC3G by impairing both its translation and intracellular stability. Mol
1267 Cell *12*, 591-601.
1268 Swingle, M., Ni, L., and Honkanen, R.E. (2007). Small-molecule inhibitors of ser/thr protein
1269 phosphatases: specificity, use and common forms of abuse. Methods Mol Biol *365*, 23-38.
1270 Vallardi, G., Allan, L.A., Crozier, L., and Saurin, A.T. (2019). Division of labour between
1271 PP2A-B56 isoforms at the centromere and kinetochore. Elife *8*.

van den Boomen, D.J., Timms, R.T., Grice, G.L., Stagg, H.R., Skodt, K., Dougan, G., Nathan, J.A., and Lehner, P.J. (2014). TMEM129 is a Derlin-1 associated ERAD E3 ligase essential for virus-induced degradation of MHC-I. Proc Natl Acad Sci U S A *111*, 11425-11430.

Wang, J., Shackelford, J.M., Casella, C.R., Shivers, D.K., Rapaport, E.L., Liu, B., Yu, X.F., and Finkel, T.H. (2007). The Vif accessory protein alters the cell cycle of human immunodeficiency virus type 1 infected cells. Virology *359*, 243-252.

Wang, J., Wang, Z., Yu, T., Yang, H., Virshup, D.M., Kops, G.J., Lee, S.H., Zhou, W., Li, X., Xu, W.*, et al.* (2016). Crystal structure of a PP2A B56-BubR1 complex and its implications for PP2A substrate recruitment and localization. Protein Cell *7*, 516-526.

Wang, Q., and Lee, C. (2007). Distinguishing Functional Amino Acid Covariation from Background Linkage Disequilibrium in HIV Protease and Reverse Transcriptase. Plos One *2*.

Wickham, H. (2009). Ggplot2 : elegant graphics for data analysis (New York: Springer).

Willey, R.L., Maldarelli, F., Martin, M.A., and Strebel, K. (1992). Human immunodeficiency virus type 1 Vpu protein induces rapid degradation of CD4. J Virol *66*, 7193-7200.

Wlodarchak, N., and Xing, Y. (2016). PP2A as a master regulator of the cell cycle. Crit Rev Biochem Mol Biol *51*, 162-184.

Yamashita, T., Kamada, K., Hatcho, K., Adachi, A., and Nomaguchi, M. (2008). Identification of amino acid residues in HIV-1 Vif critical for binding and exclusion of APOBEC3G/F. Microbes Infect *10*, 1142-1149.

Yang, J., and Phiel, C. (2010). Functions of B56-containing PP2As in major developmental and cancer signaling pathways. Life sciences *87*, 659-666.

Yu, G.C., Lam, T.T.Y., Zhu, H.C., and Guan, Y. (2018). Two Methods for Mapping and Visualizing Associated Data on Phylogeny Using Ggtree. Molecular biology and evolution *35*, 3041-3043.

Yu, X., Yu, Y., Liu, B., Luo, K., Kong, W., Mao, P., and Yu, X.F. (2003). Induction of APOBEC3G ubiquitination and degradation by an HIV-1 Vif-Cul5-SCF complex. Science *302*, 1056-1060.

Zhao, K., Du, J., Rui, Y., Zheng, W., Kang, J., Hou, J., Wang, K., Zhang, W., Simon, V.A., and Yu, X.F. (2015). Evolutionarily conserved pressure for the existence of distinct G2/M cell cycle arrest and A3H inactivation functions in HIV-1 Vif. Cell cycle *14*, 838-847.

Figure 1

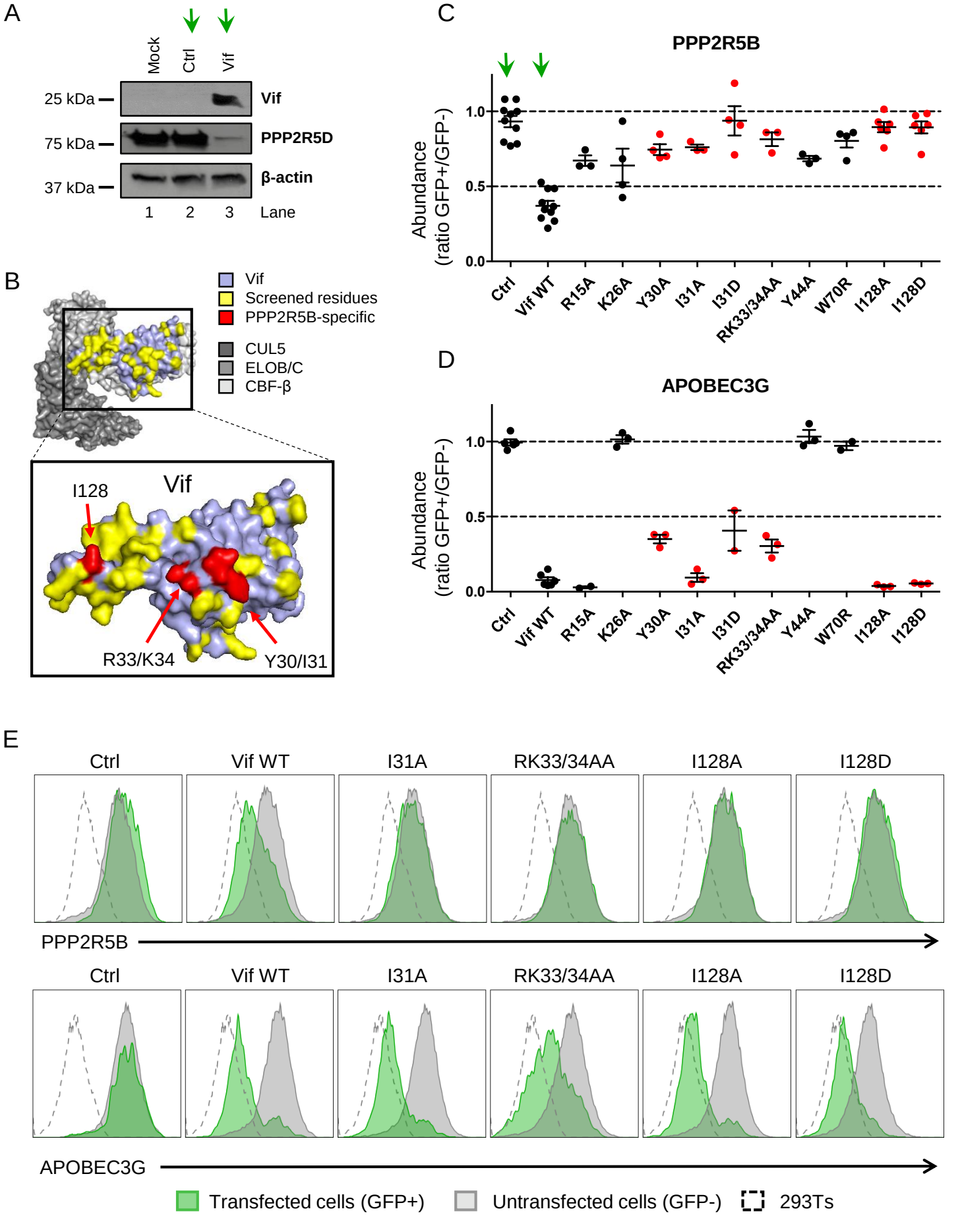
A
Mock
Ctrl
Vif
25 kDa
75 kDa
37 kDa
Vif
PPP2R5D
β-actin
1
2
3
Lane
B
Vif
Screened residues
PPP2R5B-specific
CUL5
ELOB/C
CBF-β
Vif
I128
R33/K34
Y30/I31
C
PPP2R5B
Abundance
(ratio GFP+/GFP-)
1.0
0.5
0.0
Ctrl
Vif WT
R15A
K26A
Y30A
I31A
I31D
RK33/34AA
Y44A
W70R
I128A
I128D
D
APOBEC3G
Abundance
(ratio GFP+/GFP-)
1.0
0.5
0.0
Ctrl
Vif WT
R15A
K26A
Y30A
I31A
I31D
RK33/34AA
Y44A
W70R
I128A
I128D
E
Ctrl
Vif WT
I31A
RK33/34AA
I128A
I128D
PPP2R5B
Ctrl
Vif WT
I31A
RK33/34AA
I128A
I128D
APOBEC3G
Transfected cells (GFP+)
Untransfected cells (GFP-)
293Ts

Figure 2

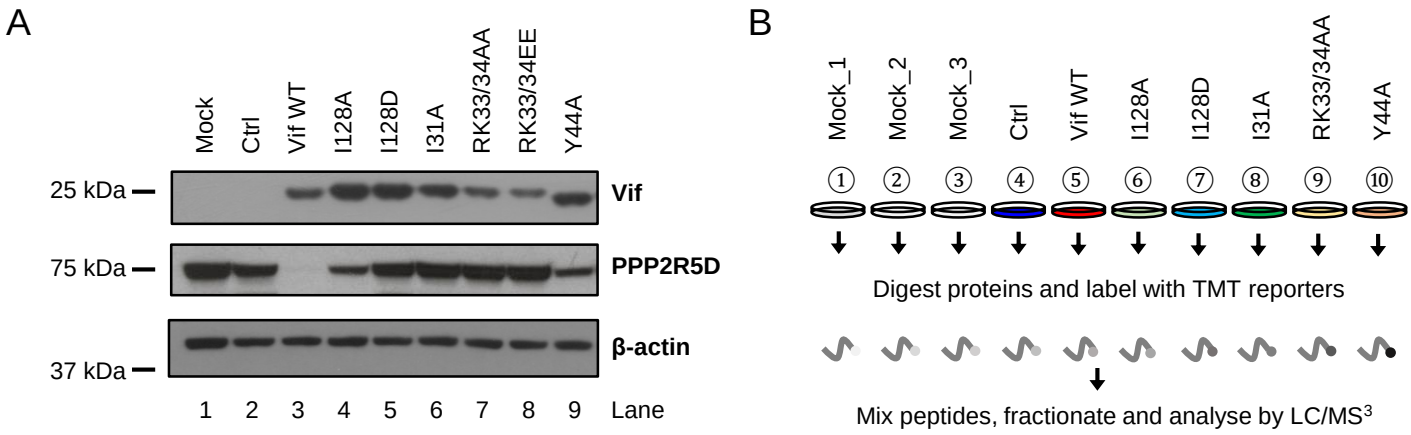
A
Mock
Ctrl
Vif WT
I128A
I128D
I31A
RK33/34AA
RK33/34EE
Y44A
25 kDa
75 kDa
37 kDa
Vif
PPP2R5D
β-actin
1 2 3 4 5 6 7 8 9 Lane
B
Mock_1
Mock_2
Mock_3
Ctrl
Vif WT
I128A
I128D
I31A
RK33/34AA
Y44A
① ② ③ ④ ⑤ ⑥ ⑦ ⑧ ⑨ ⑩
Digest proteins and label with TMT reporters
Mix peptides, fractionate and analyse by LC/MS3

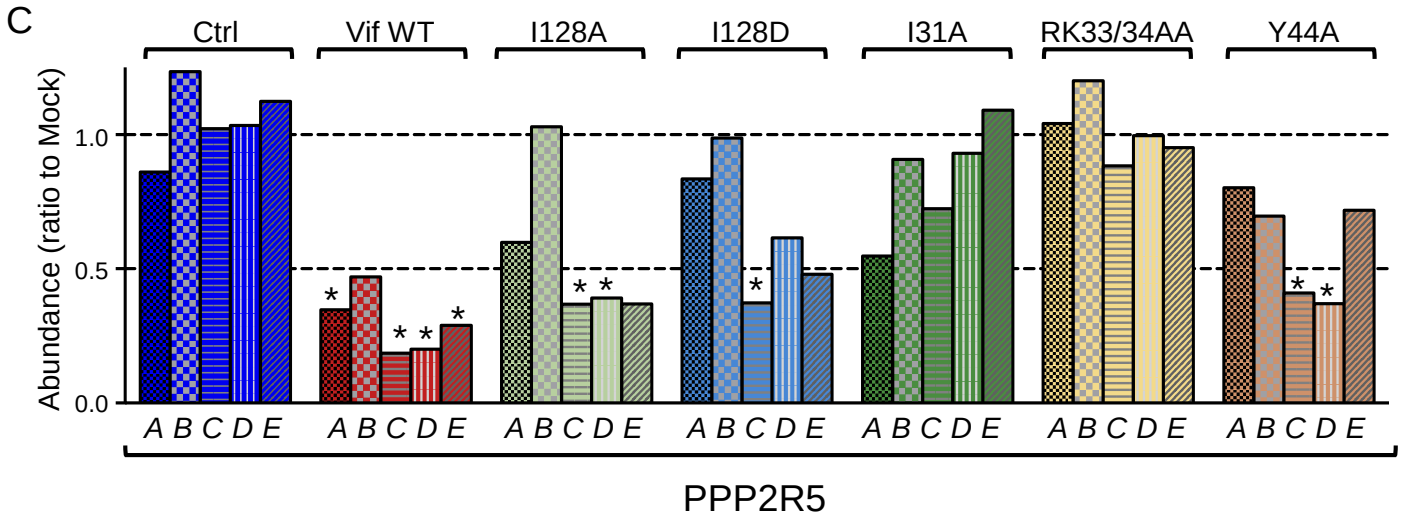
C
Ctrl
Vif WT
I128A
I128D
I31A
RK33/34AA
Y44A
Abundance (ratio to Mock)
1.0
0.5
0.0
A B C D E
PPP2R5

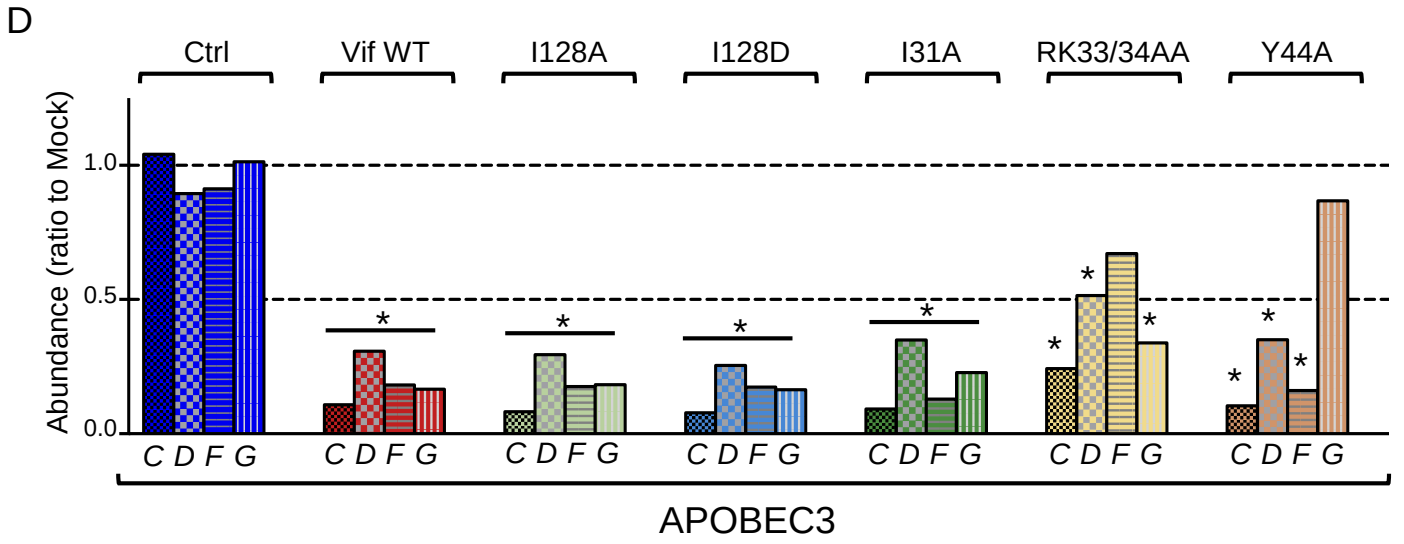
D
Ctrl
Vif WT
I128A
I128D
I31A
RK33/34AA
Y44A
Abundance (ratio to Mock)
1.0
0.5
0.0
C D F G
APOBEC3

Figure 3

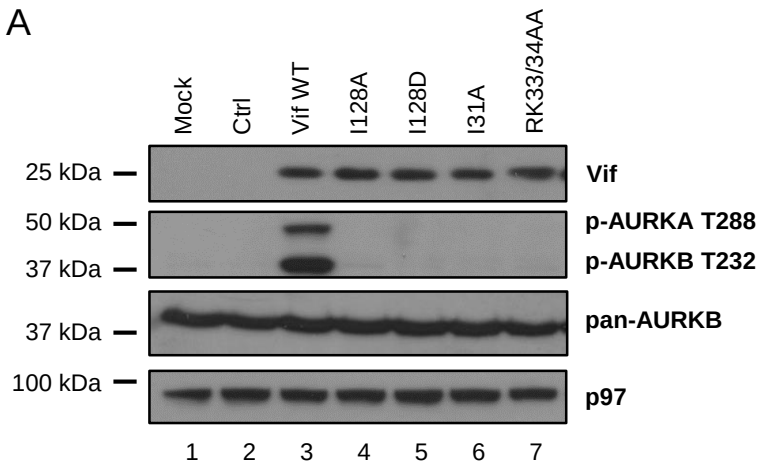
A
Mock
Ctrl
Vif WT
I128A
I128D
I31A
RK33/34AA
25 kDa
50 kDa
37 kDa
37 kDa
100 kDa
Vif
p-AURKA T288
p-AURKB T232
pan-AURKB
p97
1 2 3 4 5 6 7

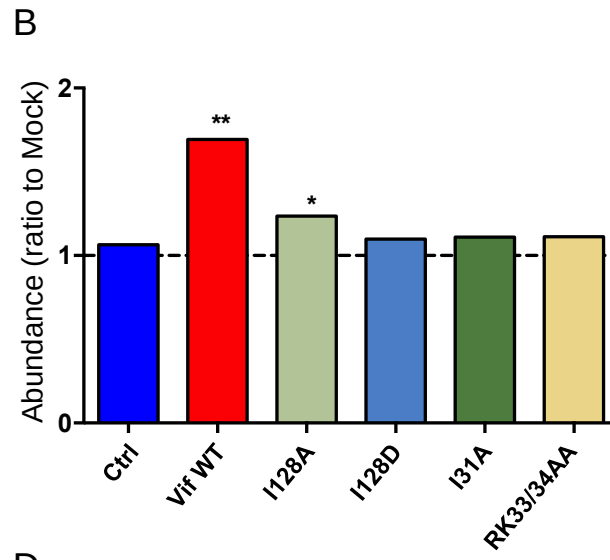
B
Abundance (ratio to Mock)
2
1
0
**
*
Ctrl
Vif WT
I128A
I128D
I31A
RK33/34AA

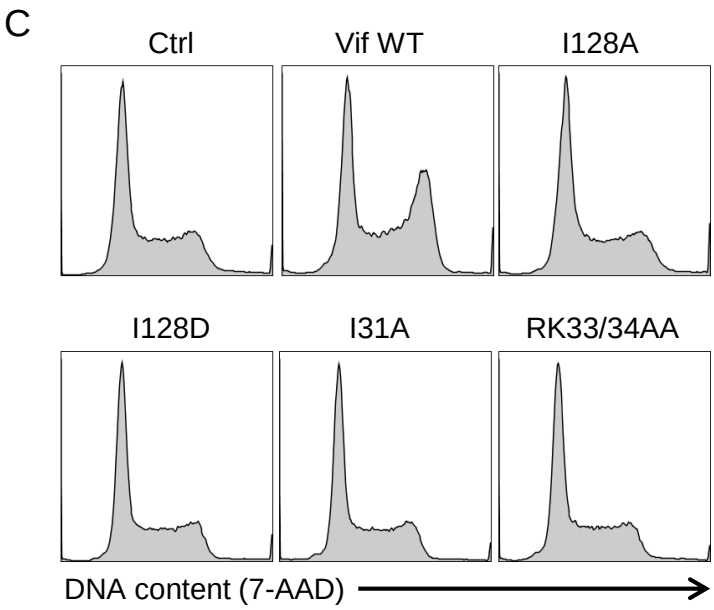
C
Ctrl
Vif WT
I128A
I128D
I31A
RK33/34AA
DNA content (7-AAD)

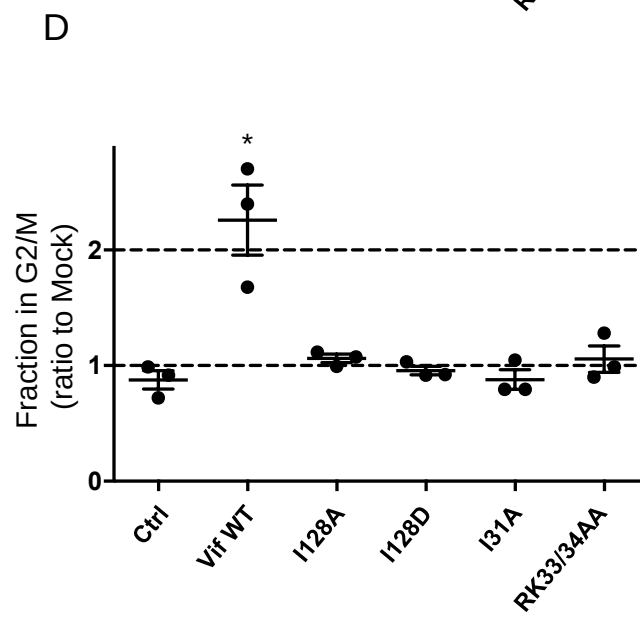
D
Fraction in G2/M
(ratio to Mock)
2
1
0
*
Ctrl
Vif WT
I128A
I128D
I31A
RK33/34AA

Figure 4

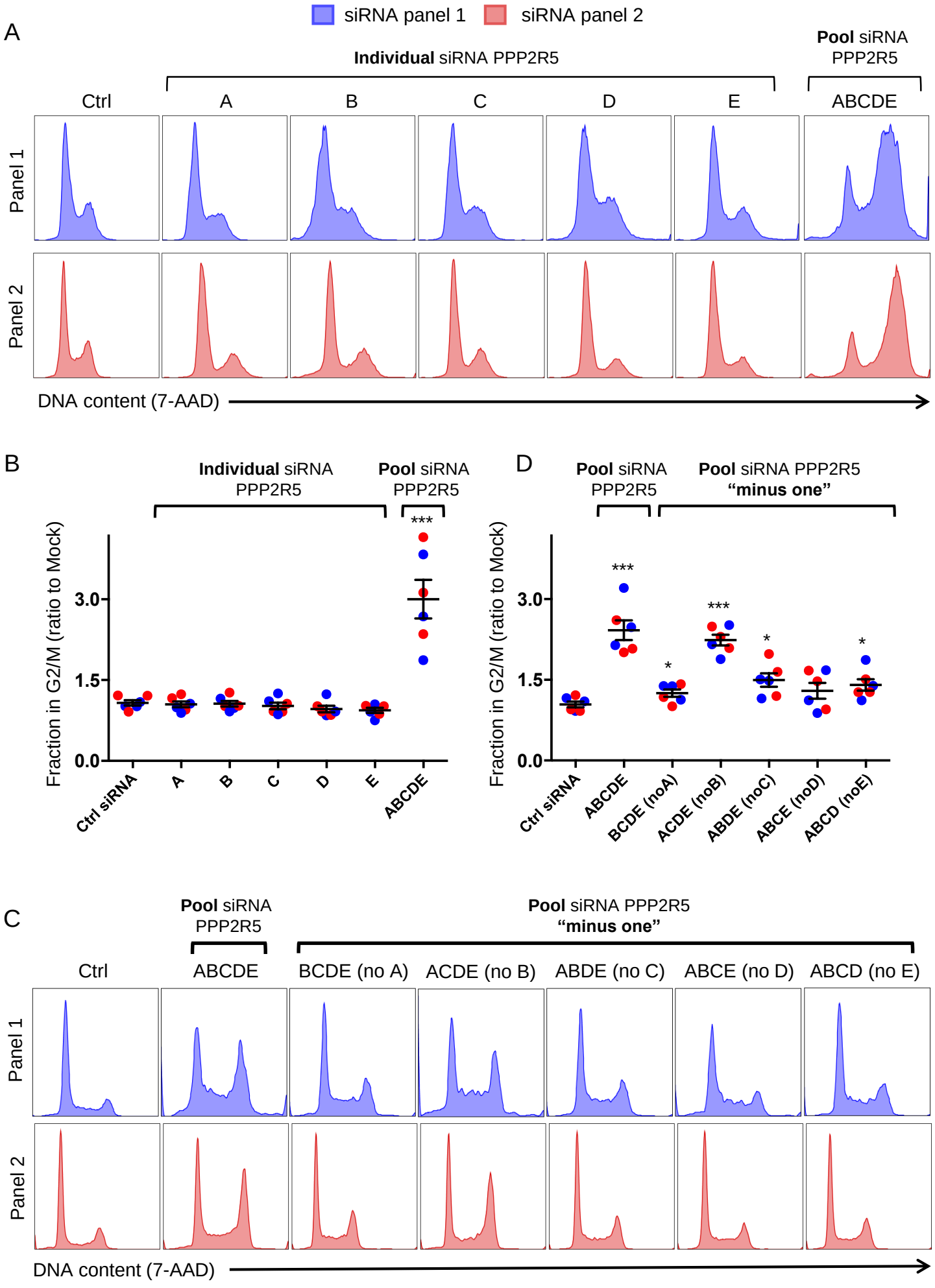
A
siRNA panel 1
siRNA panel 2
Individual siRNA PPP2R5
Pool siRNA PPP2R5
Ctrl
A
B
C
D
E
ABCDE
Panel 1
Panel 2
DNA content (7-AAD)
B
Individual siRNA PPP2R5
Pool siRNA PPP2R5
***
Fraction in G2/M (ratio to Mock)
3.0
1.5
0.0
Ctrl siRNA
A
B
C
D
E
ABCDE
D
Pool siRNA PPP2R5
Pool siRNA PPP2R5 "minus one"
***
***
*
*
*
Fraction in G2/M (ratio to Mock)
3.0
1.5
0.0
Ctrl siRNA
ABCDE
BCDE (noA)
ACDE (noB)
ABDE (noC)
ABCE (noD)
ABCD (noE)
C
Pool siRNA PPP2R5
Pool siRNA PPP2R5 "minus one"
Ctrl
ABCDE
BCDE (no A)
ACDE (no B)
ABDE (no C)
ABCE (no D)
ABCD (no E)
Panel 1
Panel 2
DNA content (7-AAD)

Figure 5

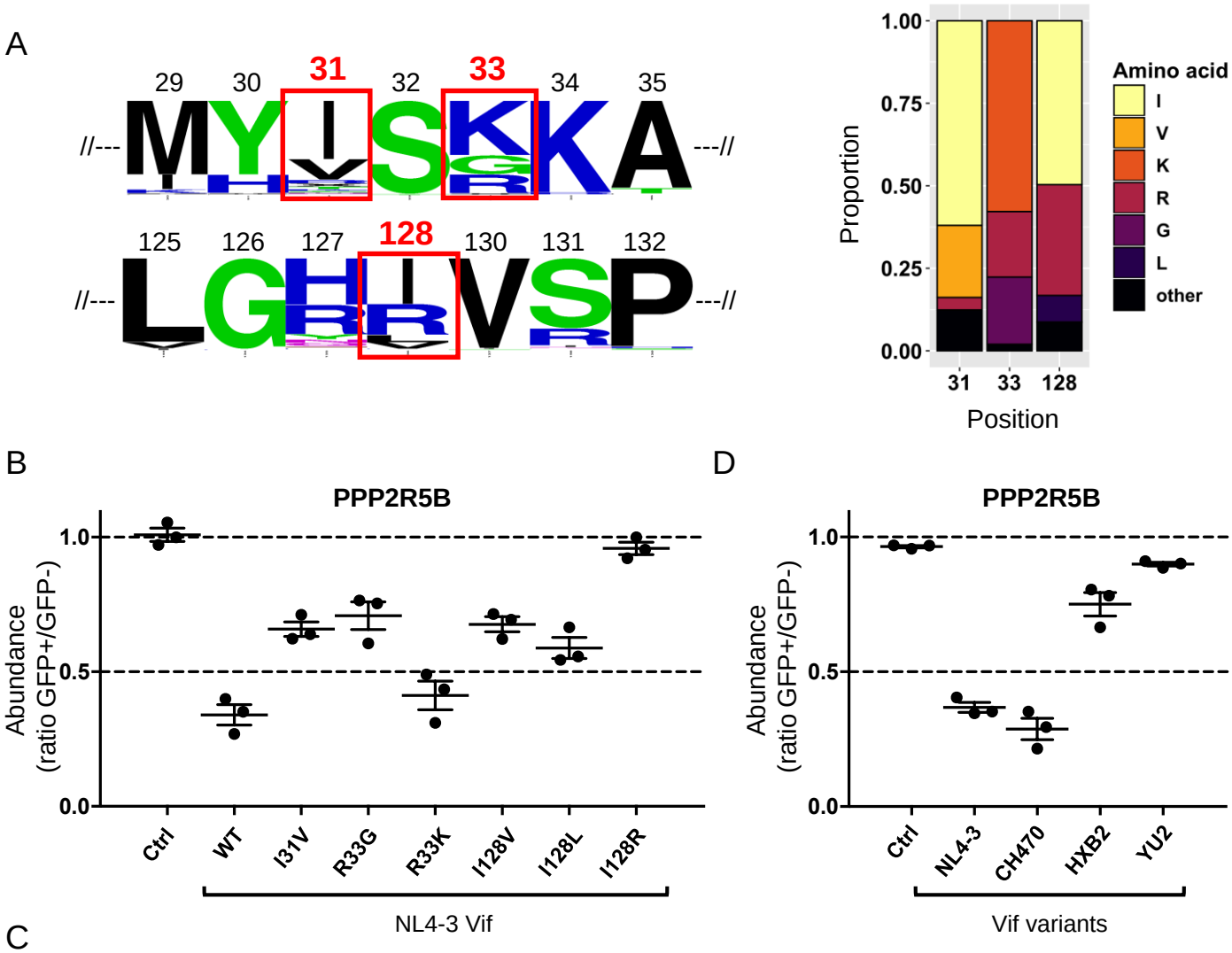
A
29 30 31 32 33 34 35
125 126 127 128 130 131 132
Proportion
Position
Amino acid
I
V
K
R
G
L
other
B
PPP2R5B
Abundance (ratio GFP+/GFP-)
Ctrl
WT
I31V
R33G
R33K
I128V
I128L
I128R
NL4-3 Vif
D
PPP2R5B
Ctrl
NL4-3
CH470
HXB2
YU2
Vif variants

C

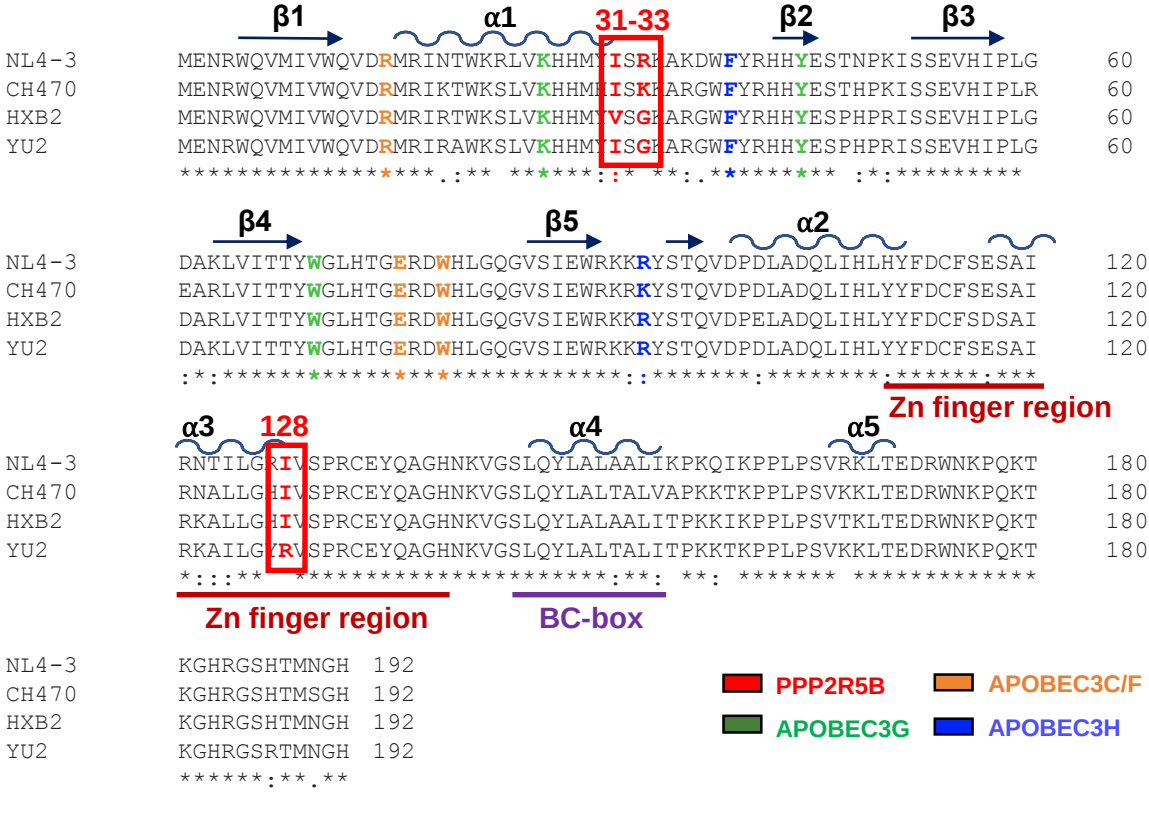
β1
α1
31-33
β2
β3
NL4-3 MENRWQVMIVWQVDRMRINTWKRLVKHHMYISRLAKDWFYRHHYESTNPKISSEVHIPLG 60
CH470 MENRWQVMIVWQVDRMRIKTWKSLVKHHMIISKLARGWFYRHHYESTHPKISSEVHIPLR 60
HXB2 MENRWQVMIVWQVDRMRIRTWKSLVKHHMYVSGLARGWFYRHHYESPHPRISSEVHIPLG 60
YU2 MENRWQVMIVWQVDRMRIRAWKSLVKHHMYISGLARGWFYRHHYESPHPRISSEVHIPLG 60
β4
β5
α2
NL4-3 DAKLVITTYWGLHTGERDWHLGQGVSIEWRKKRYSTQVDPDLADQLIHLHYFDCFSESAI 120
CH470 EARLVITTYWGLHTGERDWHLGQGVSIEWRKKRKYSTQVDPDLADQLIHLYYFDCFSESAI 120
HXB2 DARLVITTYWGLHTGERDWHLGQGVSIEWRKKRYSTQVDPELADQLIHLYYFDCFSDSAI 120
YU2 DAKLVITTYWGLHTGERDWHLGQGVSIEWRKKRYSTQVDPDLADQLIHLYYFDCFSESAI 120
Zn finger region
α3
128
α4
α5
NL4-3 RNTILGRIVSPRCEYQAGHNKVGSLQYLALAALIKPKQIKPPLPSVRKLTEDRWNKPQKT 180
CH470 RNALLGHIVSPRCEYQAGHNKVGSLQYLALTALVAPKKTKPPLPSVKKLTEDRWNKPQKT 180
HXB2 RKALLGHIVSPRCEYQAGHNKVGSLQYLALAALITPKKIKPPLPSVTKLTEDRWNKPQKT 180
YU2 RKAILGYRVSPRCEYQAGHNKVGSLQYLALTALITPKKTKPPLPSVKKLTEDRWNKPQKT 180
Zn finger region
BC-box
NL4-3 KGHRGSHTMNGH 192
CH470 KGHRGSHTMSGH 192
HXB2 KGHRGSHTMNGH 192
YU2 KGHRGSRTMNGH 192
PPP2R5B
APOBEC3C/F
APOBEC3G
APOBEC3H

Figure 6

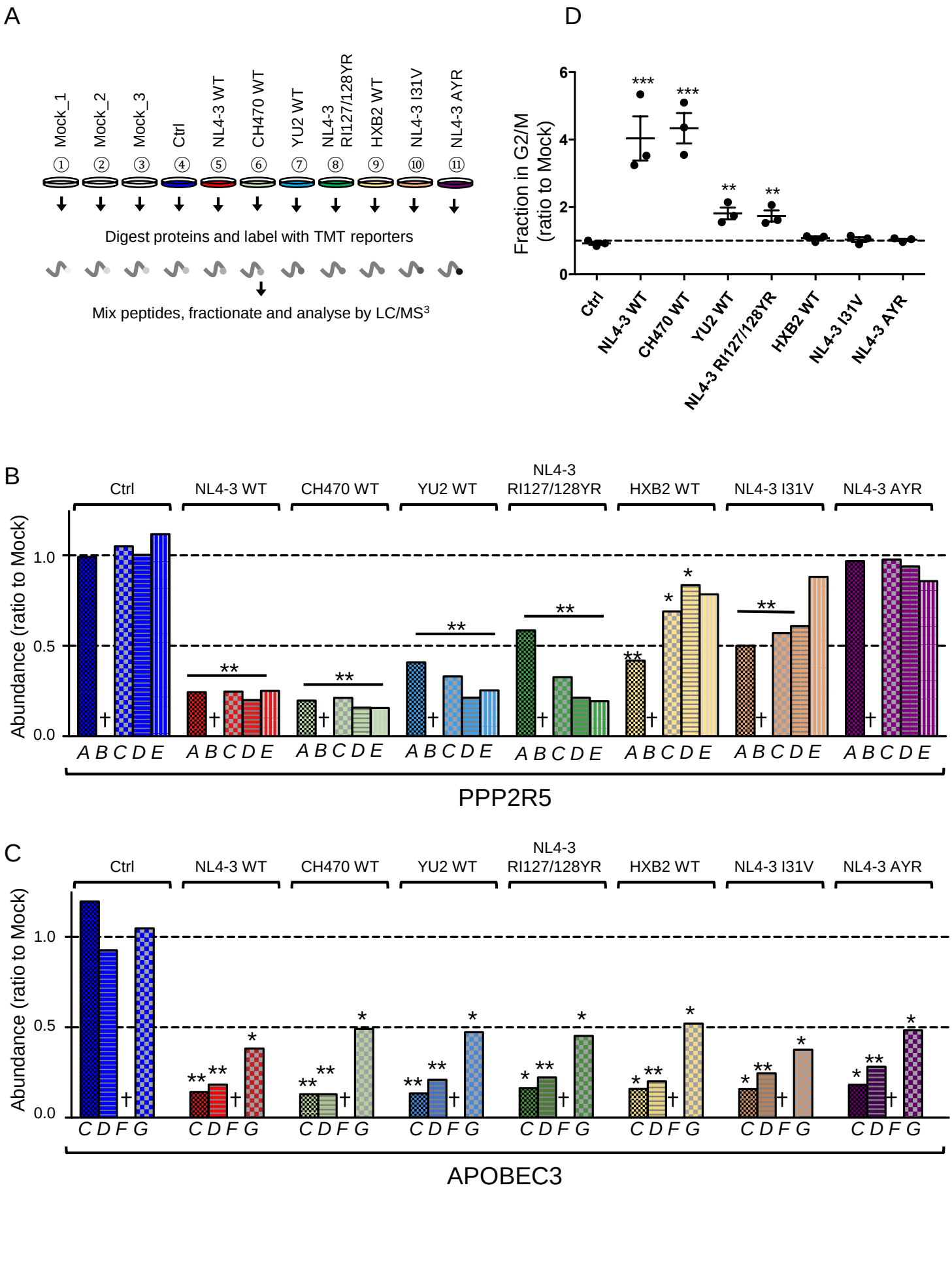
A
Mock_1
Mock_2
Mock_3
Ctrl
NL4-3 WT
CH470 WT
YU2 WT
NL4-3 RI127/128YR
HXB2 WT
NL4-3 I31V
NL4-3 AYR
① ② ③ ④ ⑤ ⑥ ⑦ ⑧ ⑨ ⑩ ⑪
Digest proteins and label with TMT reporters
Mix peptides, fractionate and analyse by LC/MS3
D
Fraction in G2/M (ratio to Mock)
Ctrl
NL4-3 WT
CH470 WT
YU2 WT
NL4-3 RI127/128YR
HXB2 WT
NL4-3 I31V
NL4-3 AYR
B
Abundance (ratio to Mock)
A B C D E
PPP2R5
C
C D F G
APOBEC3

Figure 7

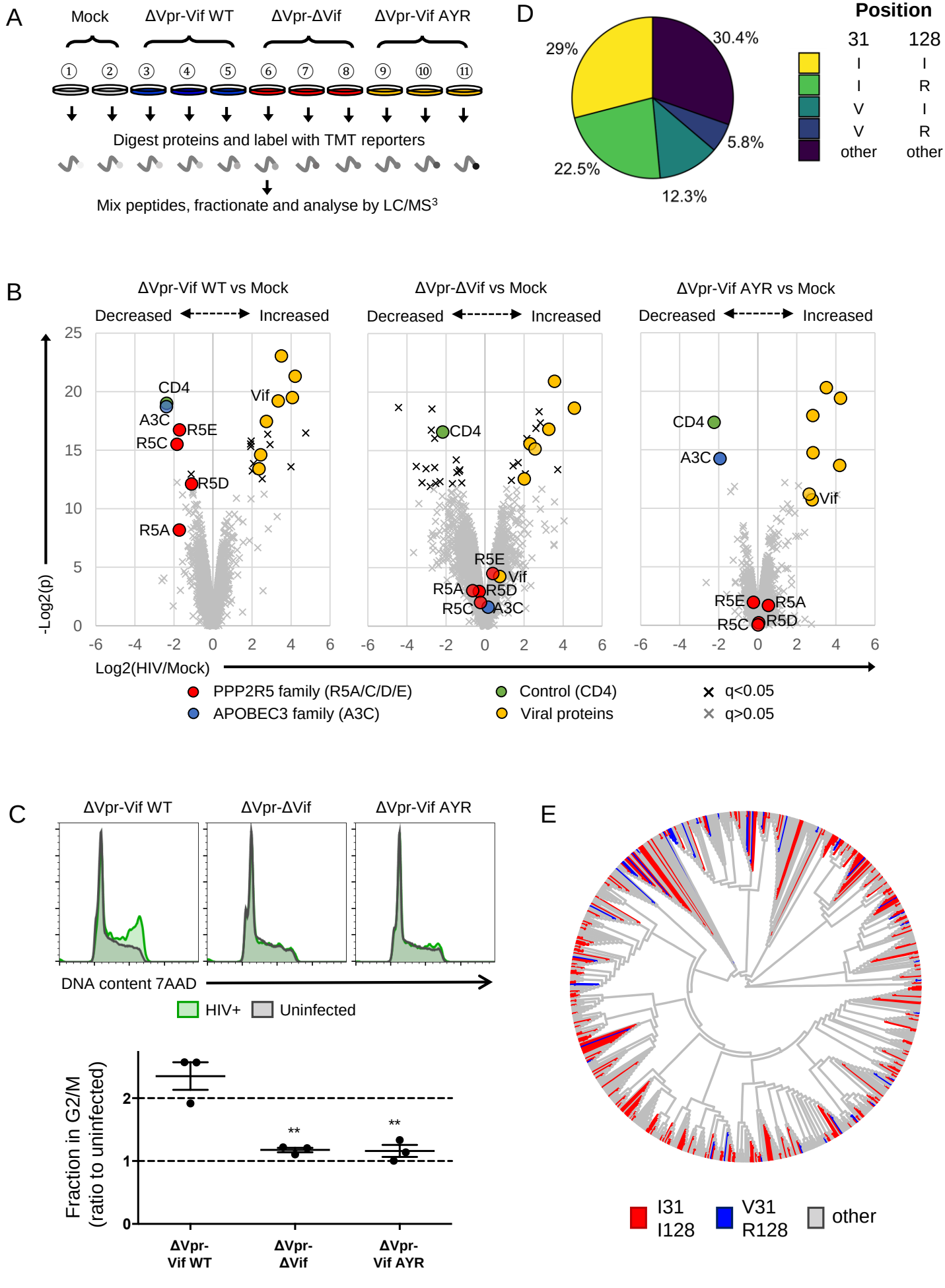
A
Mock
ΔVpr-Vif WT
ΔVpr-ΔVif
ΔVpr-Vif AYR
Digest proteins and label with TMT reporters
Mix peptides, fractionate and analyse by LC/MS3
D
Position
31
128
I I
I R
V I
V R
other other
30.4%
5.8%
12.3%
22.5%
29%
B
ΔVpr-Vif WT vs Mock
ΔVpr-ΔVif vs Mock
ΔVpr-Vif AYR vs Mock
Decreased
Increased
-Log2(p)
Log2(HIV/Mock)
CD4
Vif
A3C
R5E
R5C
R5D
R5A
PPP2R5 family (R5A/C/D/E)
APOBEC3 family (A3C)
Control (CD4)
Viral proteins
q<0.05
q>0.05
C
ΔVpr-Vif WT
ΔVpr-ΔVif
ΔVpr-Vif AYR
DNA content 7AAD
HIV+
Uninfected
Fraction in G2/M
(ratio to uninfected)
**
**
ΔVpr-
Vif WT
ΔVpr-
ΔVif
ΔVpr-
Vif AYR
E
I31
I128
V31
R128
other

Figure 1–figure supplement 1

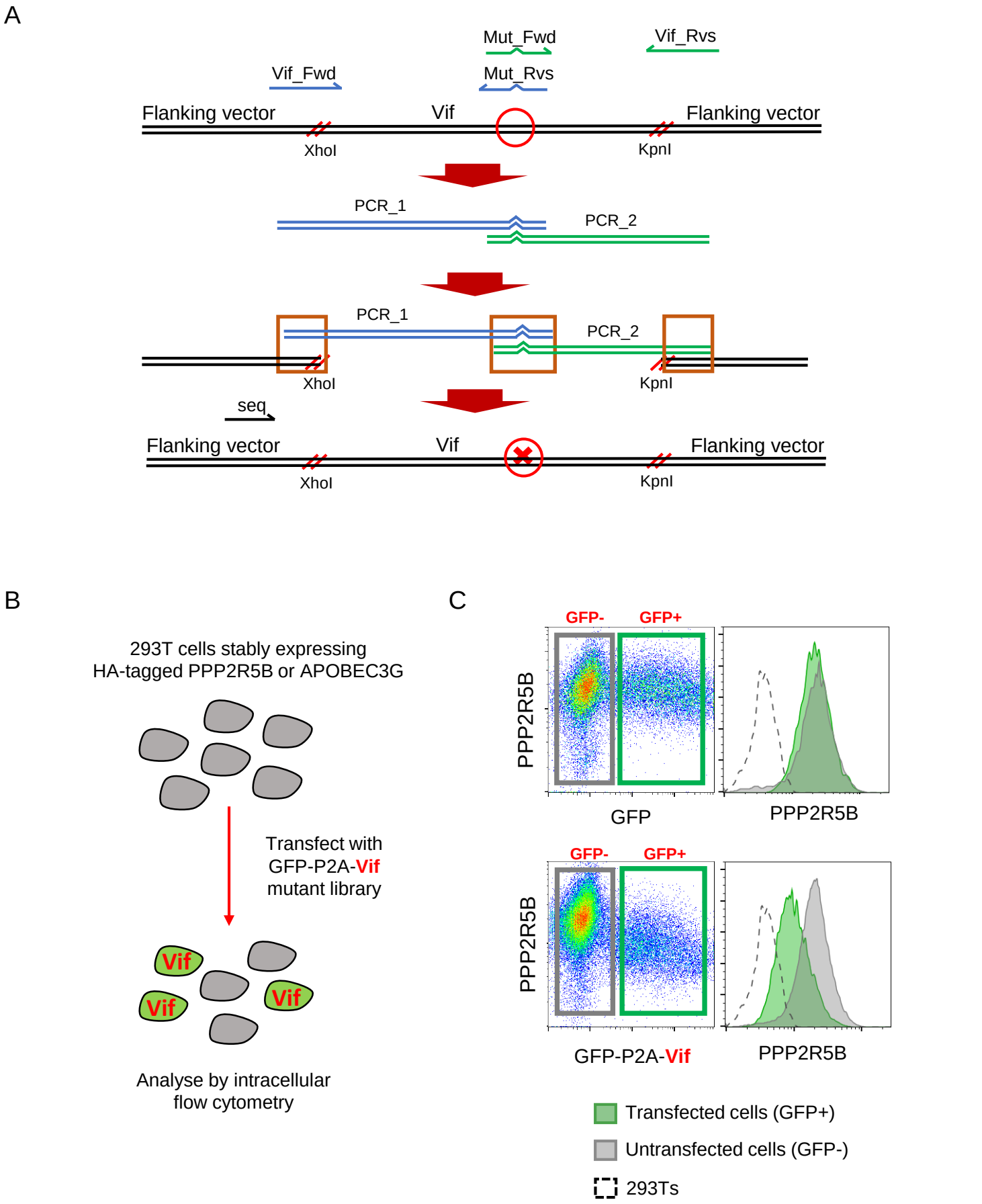

Figure 1–figure supplement 2

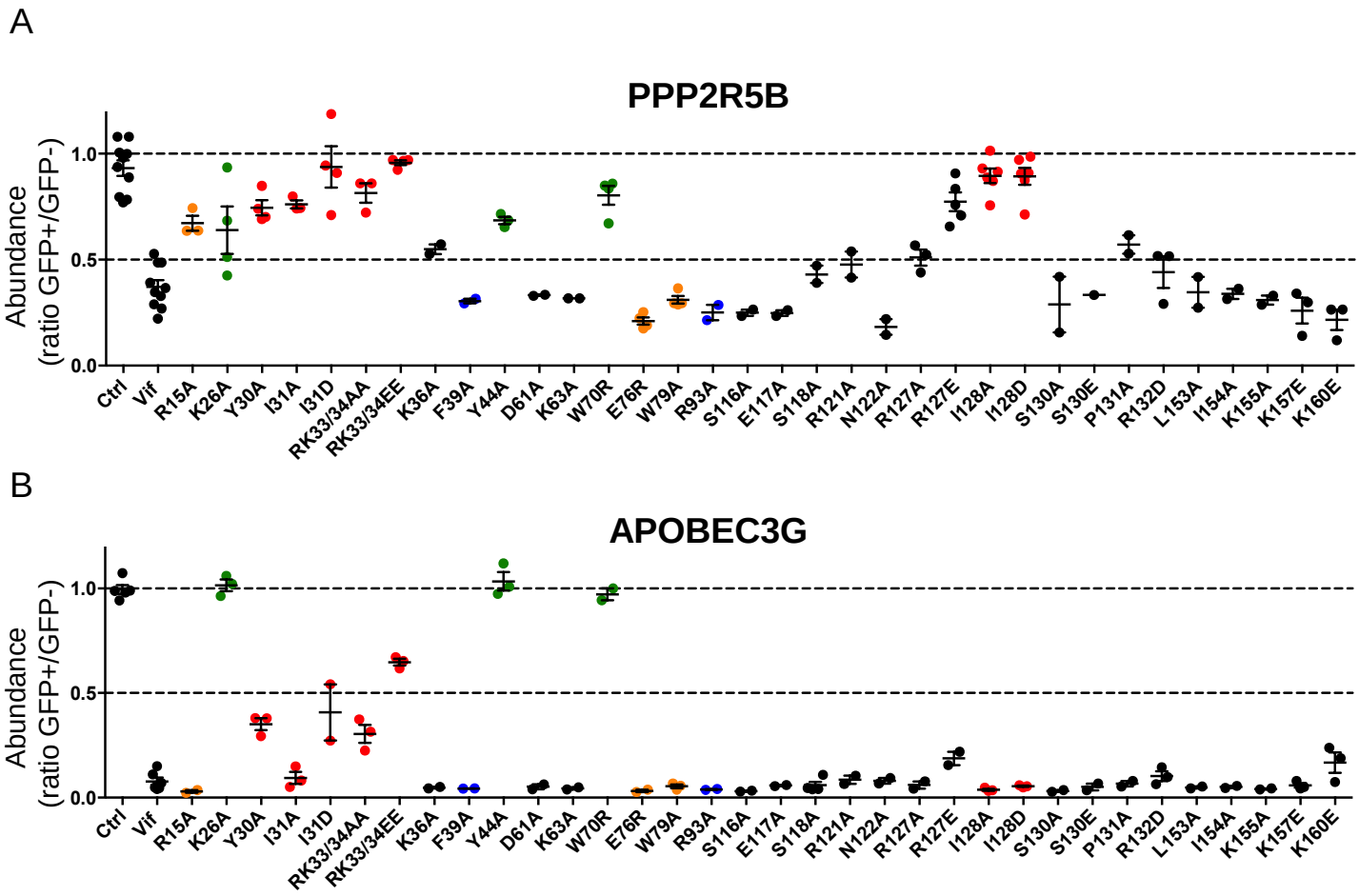

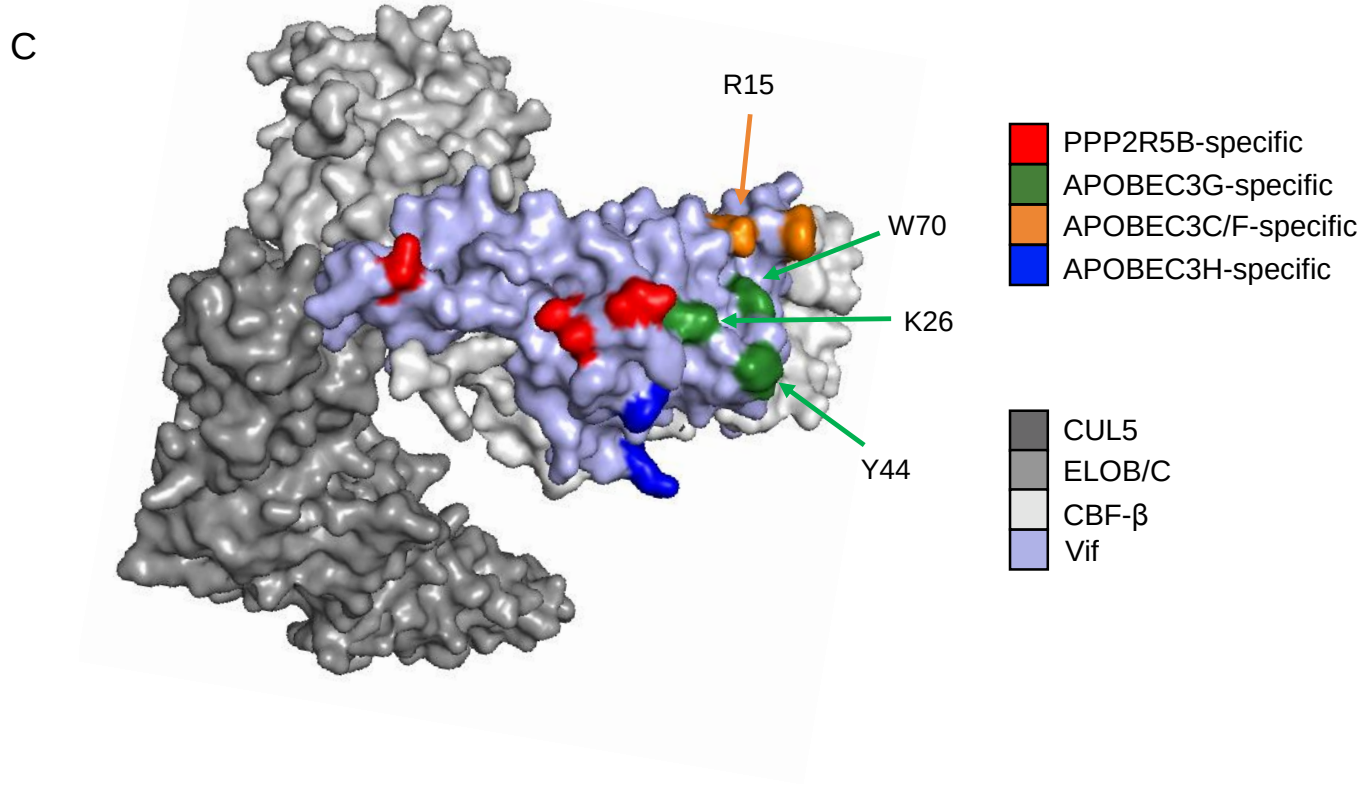

Figure 2–figure supplement 1

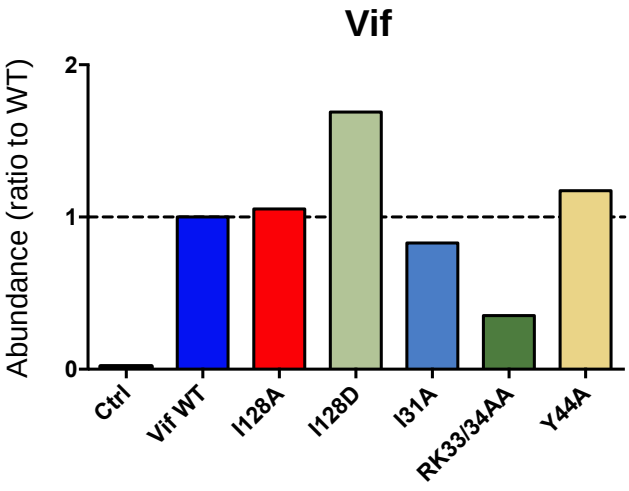

Figure 2–figure supplement 2

PPP2R5A

- Mock
- **Ctrl**
- **Vif WT**

PPP2R5A protein abundance (normalized, unscaled)						
Mock					**Ctrl**	**Vif WT**
Mock_1	Mock_2	Mock_3	*Mean* ($\bar{x}$)	*St. dev.* (*S*)		
1915	1696	2125	*1912*	*214*	1647	665

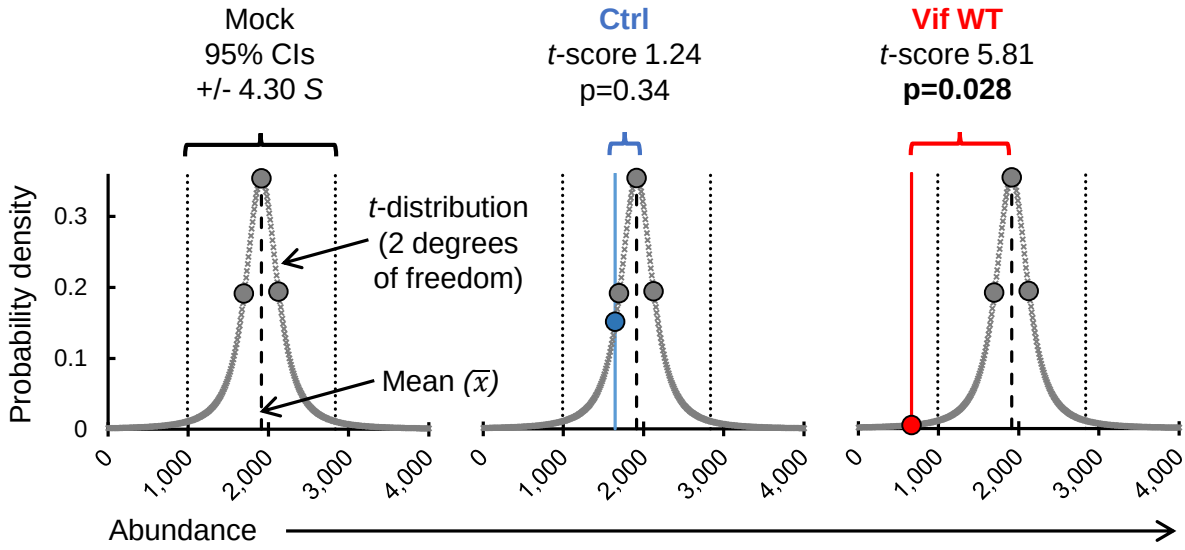

Figure 3–figure supplement 1

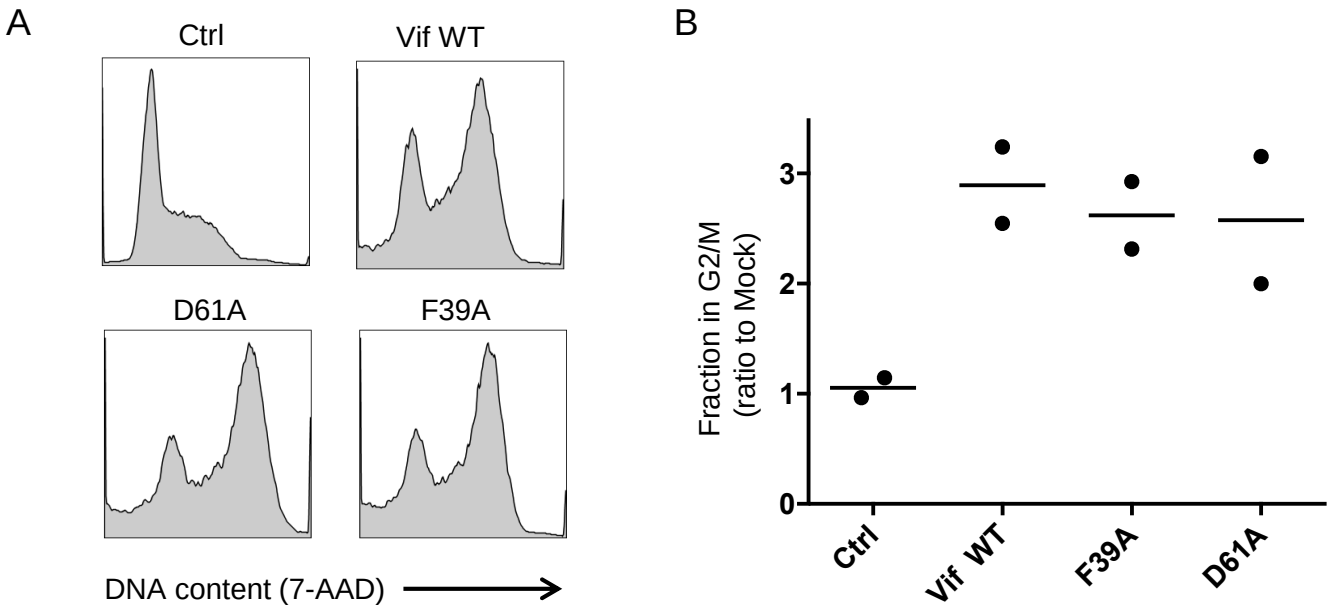

Figure 3–figure supplement 2

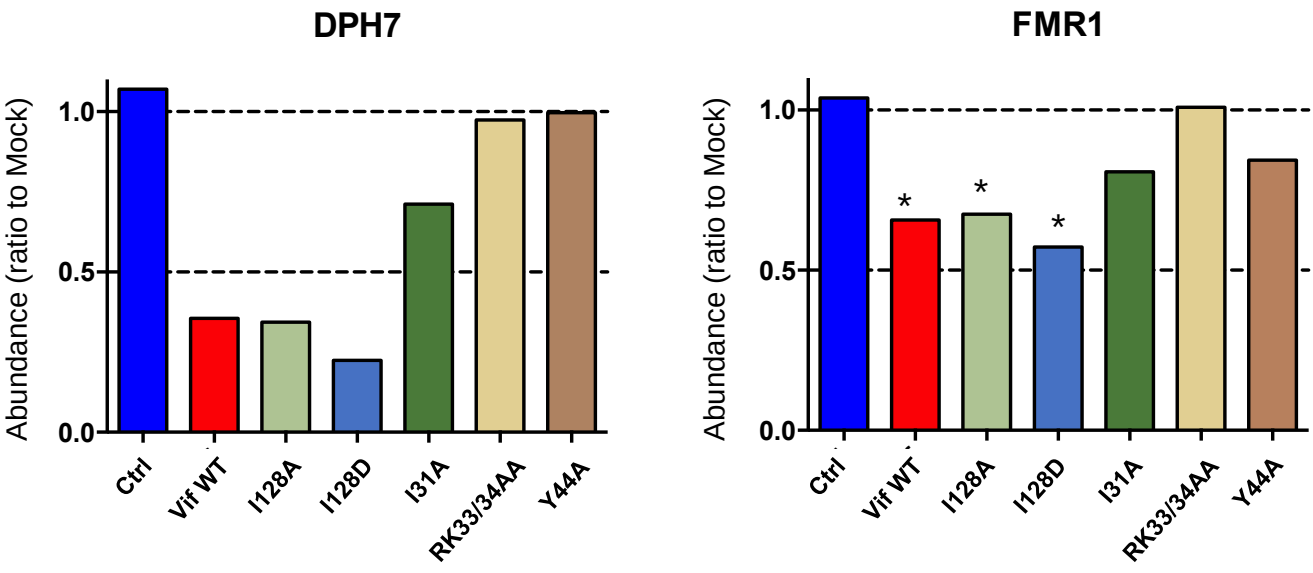

Figure 4–figure supplement 1

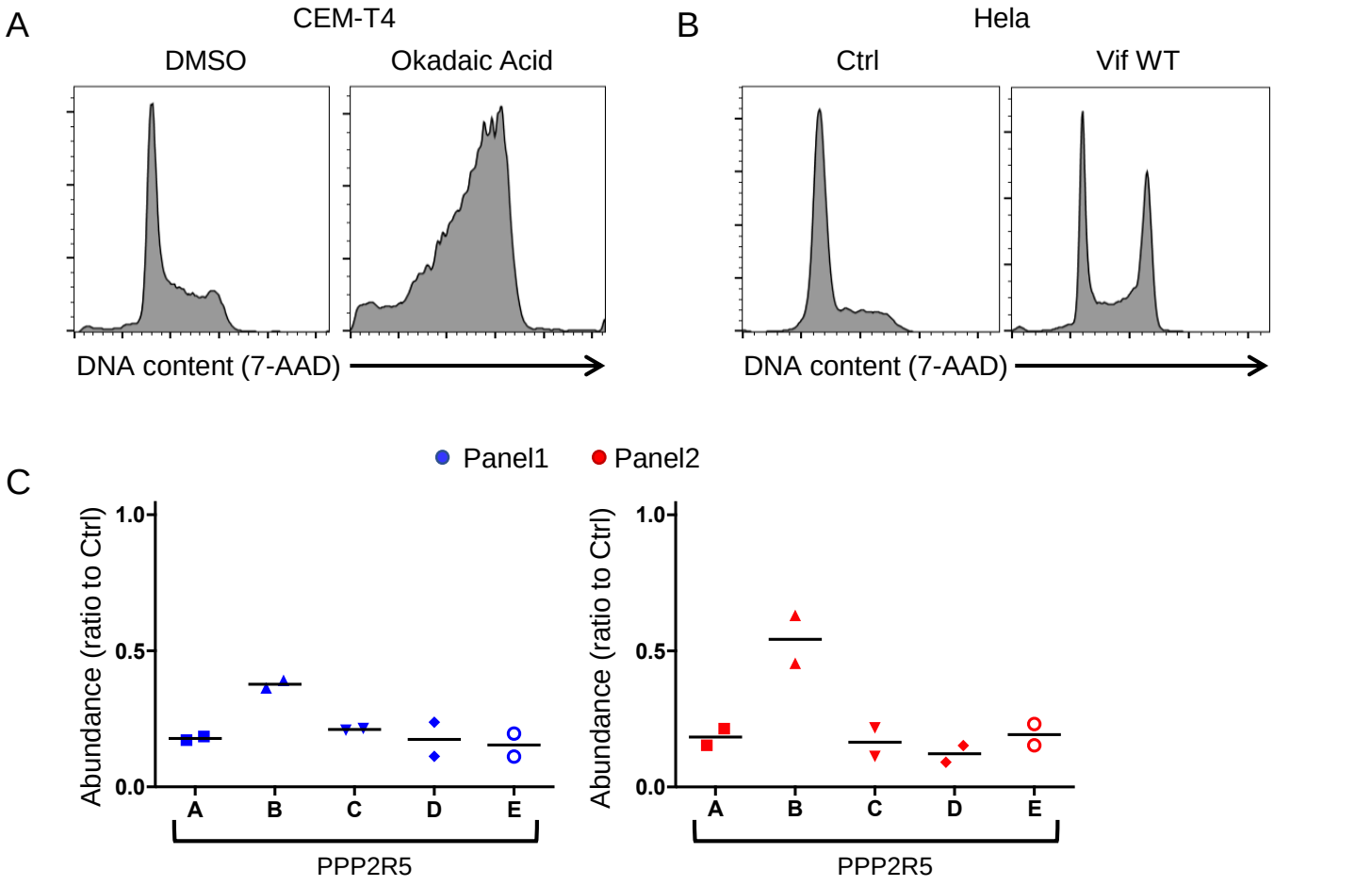

Figure 4–figure supplement 2

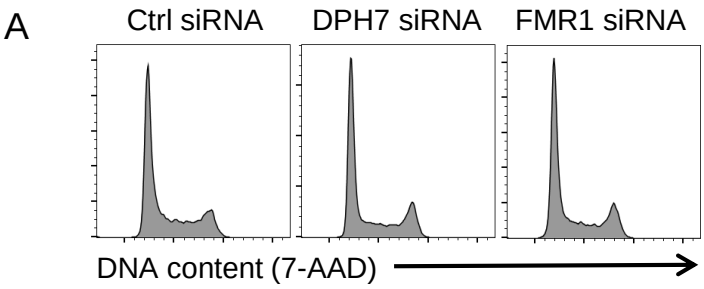

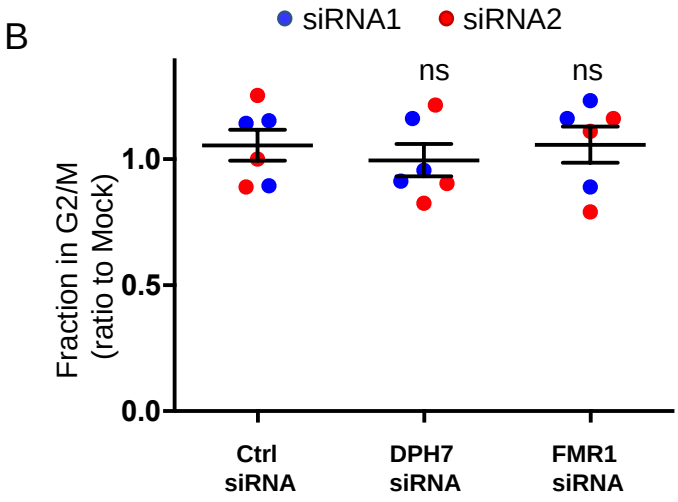

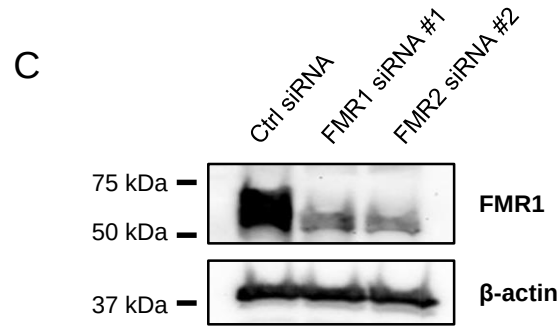

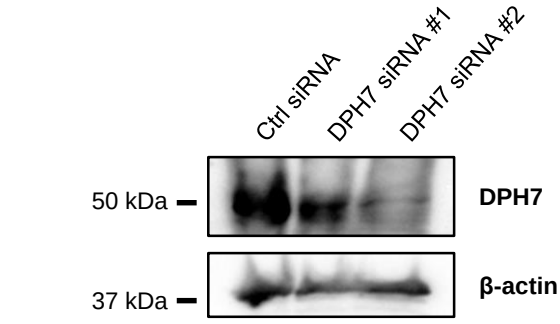

Figure 5–figure supplement 1

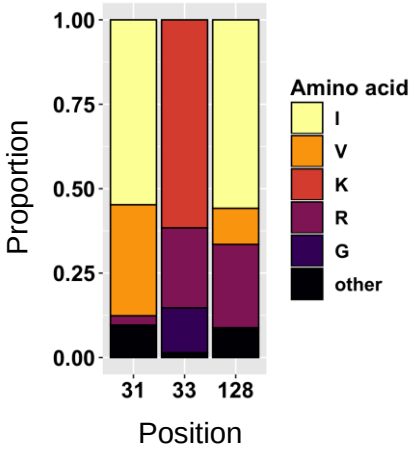

Figure 5–figure supplement 2

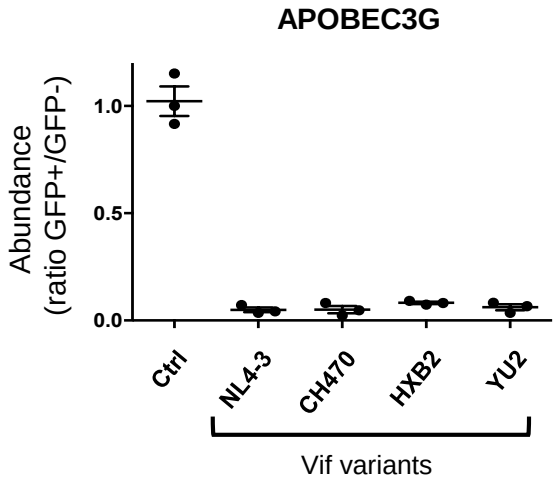

Figure 6–figure supplement 1

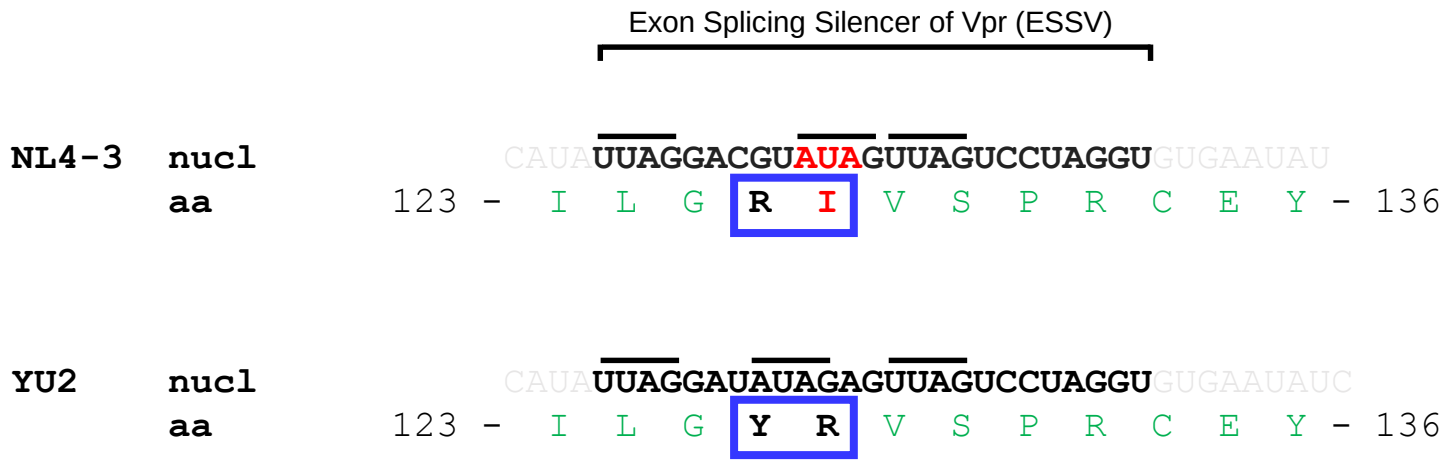

Figure 6–figure supplement 2

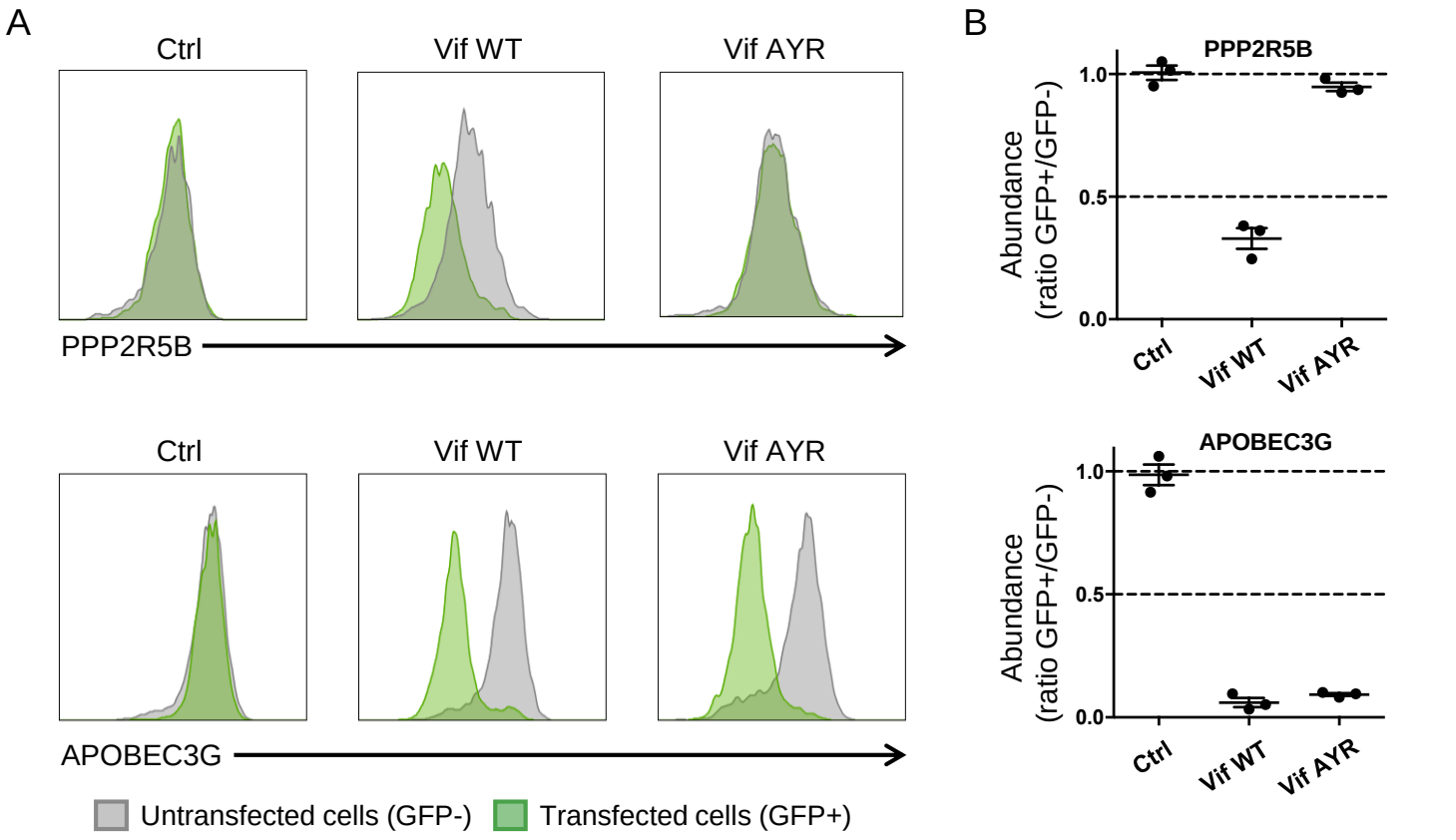

Figure 6–figure supplement 3

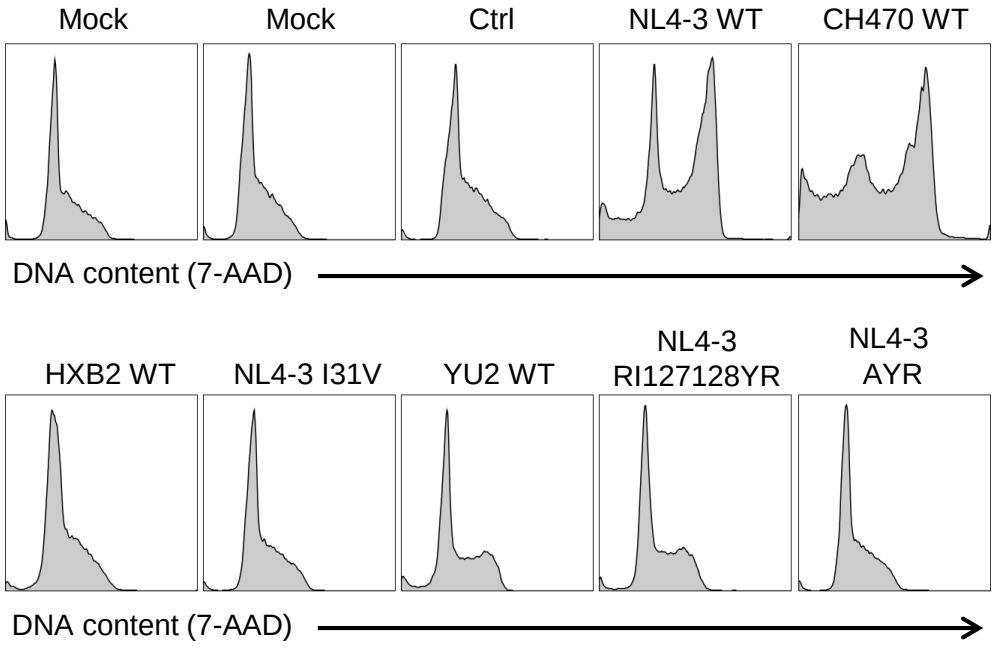

Figure 7–figure supplement 1

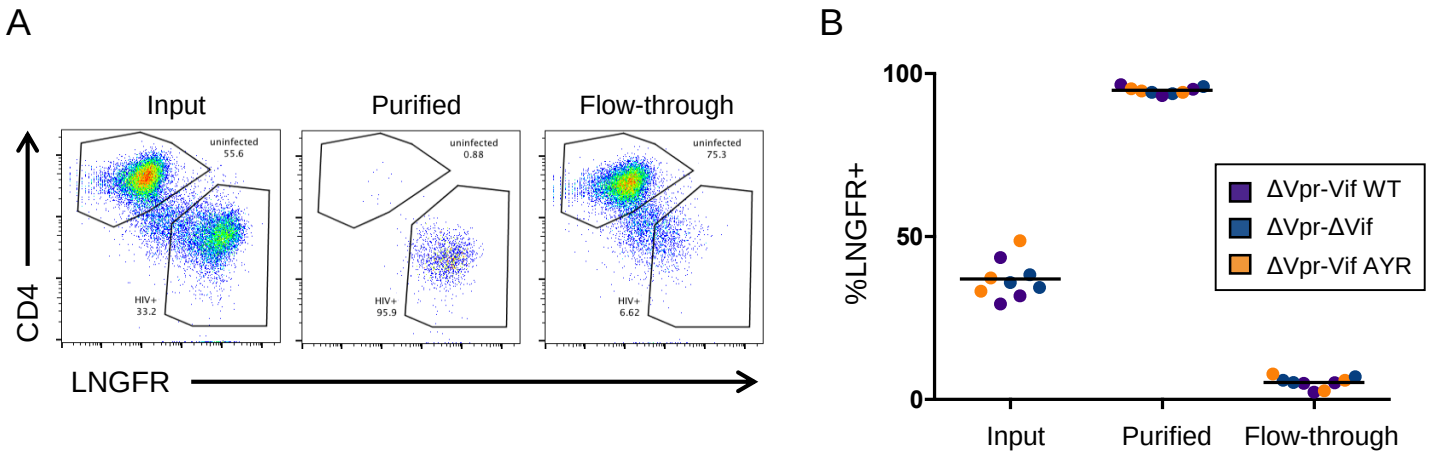

Figure 7–figure supplement 2

A

Position 31	Position 128: not R	R	Total
not V	1094	603	1697
V	348	126	474
Total	1442	729	2171

Fisher's exact test: p=0.0003

Position 31	Position 128: I	R	Total
I	630	488	1118
V	267	126	393
Total	897	614	1511

Fisher's exact test: p<0.0001

B

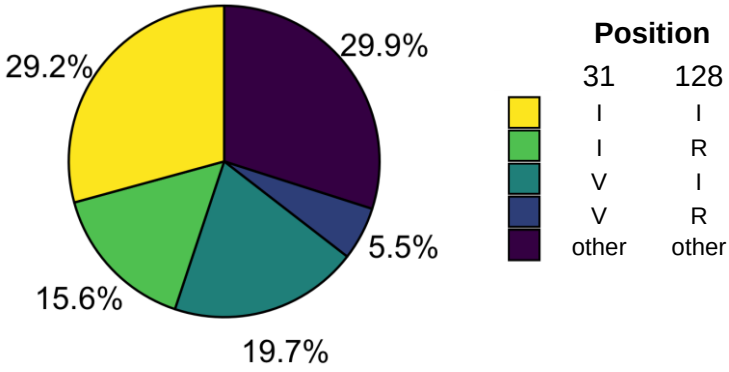

C

Position 31	Position 128: not R	R	Total
not V	1637	653	2290
V	933	189	1122
Total	2570	842	3412

Fisher's exact test: p<0.0001

Position 31	Position 128: I	R	Total
I	998	533	1531
V	671	189	860
Total	1669	722	2391

Fisher's exact test: p<0.0001

Figure 7–figure supplement 3